"BABES-BOLYAI" UNIVERSITY, FACULTY OF PHYSICS

"IULIU HATIEGANU" UNIVERSITY OF MEDICINE AND PHARMACY, FACULTY OF MEDICINE

ROZALIA VERES

Structure and properties of new systems of biomedical interest

PhD Thesis Summary

Scientific Supervisors:
Prof. Dr. Viorica SIMON
Prof. Dr. Constantin CIUCE

Cluj-Napoca, 2013

“BABES-BOLYAI” UNIVERSITY, FACULTY OF PHYSICS
“IULIU HATIEGANU” UNIVERSITY OF MEDICINE AND PHARMACY,
FACULTY OF MEDICINE

Structure and properties of new systems of biomedical interest

PhD Thesis Summary

PhD Candidate:
Rozalia VERES

Scientific Supervisors:
Prof. Dr. Viorica SIMON
Prof. Dr. Constantin CIUCE

Cluj-Napoca, 2013

Contents

Introduction

The purpose of this thesis is to synthesize and characterize new materials prepared by the sol-gel method with properties tailored for biomedical applications in tissue engineering. Bioactive glasses have attracted significant attention in the last decades, and in last years they were frequently included as inorganic phases in composite biomaterials designed as scaffolds in tissue engineering. These biomaterials have also been used in clinical applications as coatings for implants, bone filling and, in a porous form, for bone regeneration [1-5]. Therefore the thesis is focused on the obtaining and characterization of bioactive glass thin films, mesoporous bioactive glasses with and without polyethylene-glycol and also macroporous, interconnected three-dimensional glass-ceramics scaffolds.

Zinc oxide addition to the phosphosilicate matrix was considered because it is known that zinc stimulates cell proliferation, as demonstrated *in vitro* and confirmed *in vivo* [6, 7]. The sol-gel technique was chosen because, in comparison with the melting method, it offers a better chemical homogeneity, low-temperature processing and also allows the control of the chemical pore size distribution [8]. An alternative approach that influences the structure and morphology of materials is the incorporation of the polyethylene-glycol (PEG) in sols during the samples synthesis.

The thesis is divided into four chapters, followed by general conclusions, list of figures, list of tables and annex. The first chapter deals with fundamental issues of bioactive glasses and glass-ceramics for tissue engineering, describing the role of zinc and PEG in the prepared glasses and also, the importance of the porosity for these systems. The second chapter describes the sol-gel method and sacrificial template method in order to obtain macroporous samples. The experimental methods and devices used for sample synthesis and their characterization are presented in the third chapter. The fourth chapter describes the obtained experimental results and the discussions on them.

2. EXPERIMENTAL RESULTS OF AFM INVESTIGATION OF SiO_2-ZnO-P_2O_5 THIN FILMS

2.1 Samples preparation

The new 44.5SiO_2-11ZnO-44.5P_2O_5 (mol %) bioglass system was prepared following the sol-gel route. The precursors used were TEOS ($Si(OC_2H_5)_4$), zinc nitrate hexahydrate ($Zn(NO_3)_2 \cdot 6H_2O$) and dibasic ammonium phosphate ($(NH_4)_2HPO_4$). The catalyst used was HNO_3. A part of the gel was used to obtain thin films (a volume of 125 µl /layer) with a Single Wafer Spin Processor (WS-400B-6NPP/LITE) on a quartz substrate and it was rotate at 1500 rot/min. Other part of gel was dried for 24 hr at 100º C.

2.2 Samples characterization by thermal analysis

The surface of the film obtained by spin-coating technique looked to be homogeneous and smooth. The TGA/DTA curves of 100°C dried sample are shown in Figure 2.1.

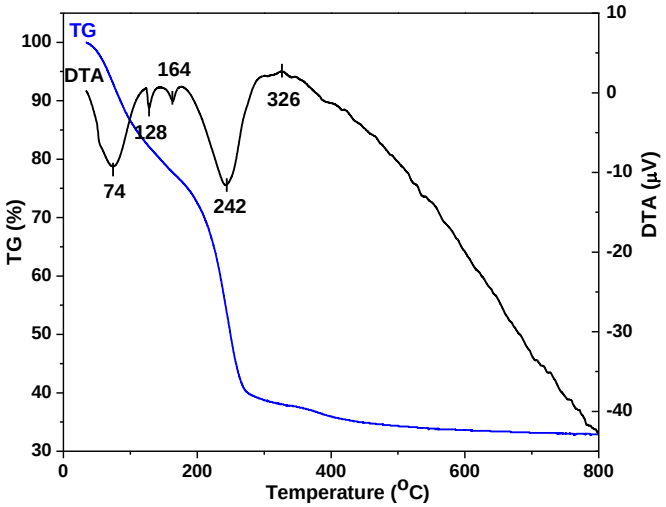

Figure 2.1 DTA and TGA runs of so-gel derived SiO_2-ZnO-P_2O_5 bioactive glass

The TGA curve presents four regions of weight loss. The first weight loss occurs in the range of 35-123ºC (17.03%) and coincides with an endothermic peak in DTA that can be associated with the remove of free water molecules. The range of 123-203º where the weight loss is about 11% presents two endothermic peaks and it can be related to the remove of water molecules physically adsorbed onto sample surface. A third weight loss (33%) can be observed in the range of 203-297 ºC with a large corresponding endothermic peak in the DTA curve. This loss can be associated with the elimination of water caged in the pores. In the fourth range (330-500ºC) it is a small weight loss (3%) and the DTA signal is diminished constantly than can correspond to the elimination of the nitrates from precursors.

2.3 Structural characterisation by X-Ray diffraction

The XRD patterns of the thin film and 100 °C dried bioactive glass sample are illustrated in Figure 2.2. The thin film XRD pattern shows a good agreement with the treated sample pattern (Bragg angle, 2θ of the peaks are similar for the two patterns with a little difference in intensity). A prevalent amorphous state of both samples can be observed. Beside the large diffraction peak that dominates the XRD pattern, there are peaks indicating the presence of a minor crystalline structure that could be assigned primary to residual nitrate or phosphate crystals. On the other hand, it is to mention that crystallites of $ZnSiO_3$, Zn_2SiO_4 and $Zn_2P_2O_7$ type have not to be completely excluded, because they could contribute to reflections very close to the same diffraction angles. Using the Scherrer equation, the crystallites size was estimated about 32.65 nm.

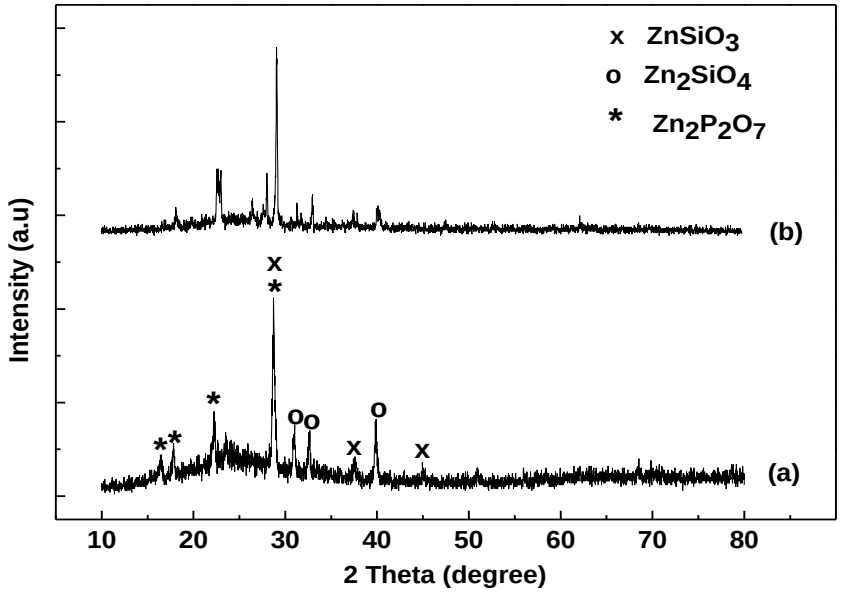

Figure 2.2 XRD pattern of SiO_2-ZnO-P_2O_5 thin film (a) and 100ºC dried sol-gel sample (b).

2.4 Morphological characterisation by Atomic Force Microscopy

Surface morphology is well revealed in AFM images. The two-dimensional (2D) and three-dimensional (3D) views of the surface morphology of thin film (scale of 15µm x 15µm) are shown in Figure 2.3.a and Figure 2.4, respectively. Their analysis denotes a rough surface that is preferred for the attachment of biomolecules.

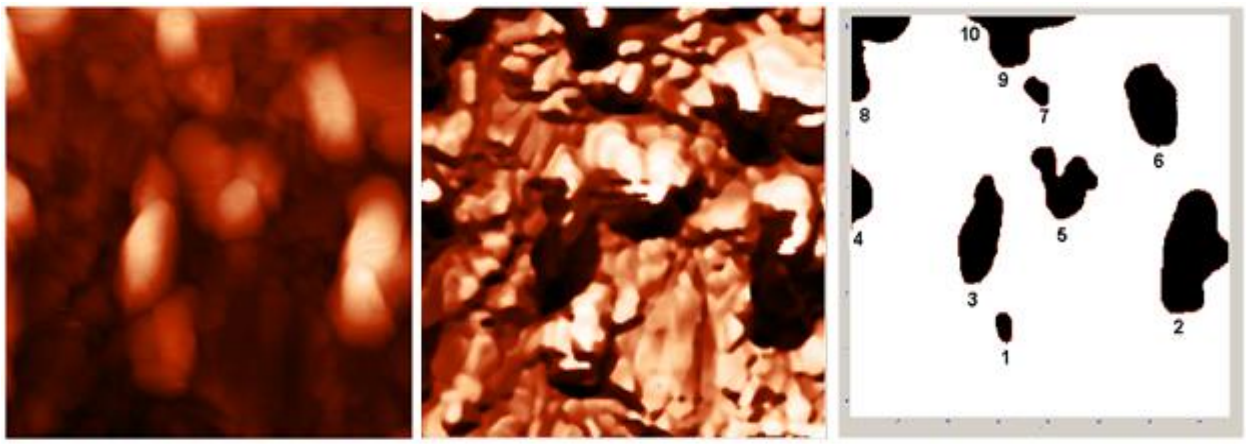

(a) (b) (c)

Figure 2.3 AFM tapping mode 2D-image (a), phase image (b), and the corresponding grains collected (c) of thin film sample.

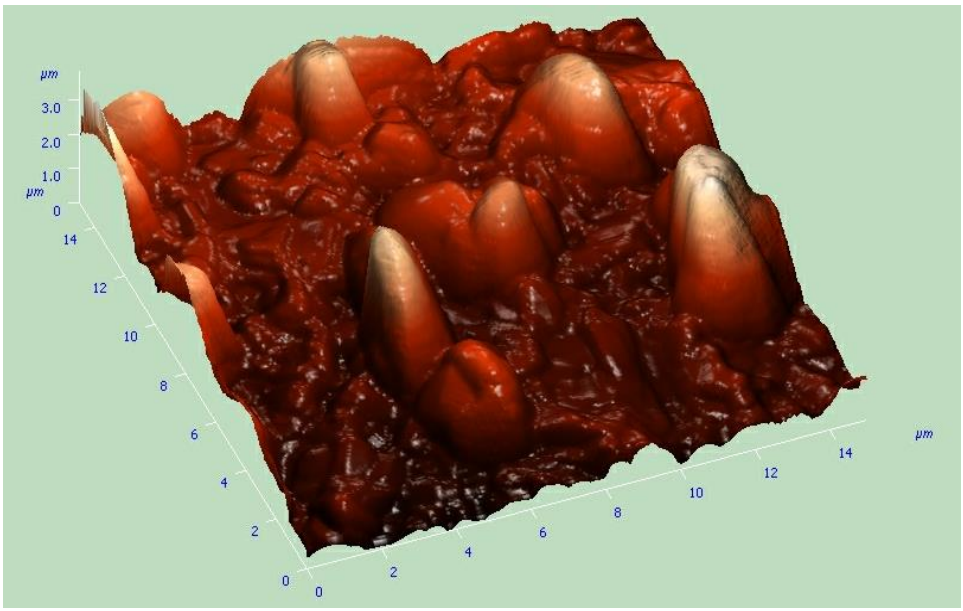

Figure 2.4 AFM tapping mode 3D-image.

AFM tapping mode allows also to display the phase image (Fig. 2.3.b) and the grain identification (Figure 2.3.c). The main geometric parameters are calculated for each separate roughness. Some characteristics of the grains were obtained using the software of the atomic force microscope. The parameters including the grain area, equal to the section area, the grain volume and maximal size, the maximal and average heights, the perimeter, along with major geometric characteristics for each grain are summarized in Table 2.1. Figure 2.5 shows the histogram of the grain area distribution density. The area of half of the gains is between 3 and 4.5 μm^2.

Table 2.1 The parameters of the grains depicted in Figure 2.3.c.

	Area, µm^2	Vol. µm^3	Z Range, µm	Max Z, µm	Mean Z, µm	Perim. µm	Diam, µm	Length µm	Mean width, µm	X Size, µm	Y Size, µm
Mean	3.253	7.056	0.787	2.458	2.023	8.176	1.824	3.176	0.824	1.882	2.471
SD	2.502	0.011	0.548	2.042	2.102	4.412	0.882	1.588	0.412	1.176	1.294
1	0.578	0.986	0.073	1.744	1.707	3.118	0.882	1.294	0.471	0.647	1.118
2	8.630	20.35	1.468	3.139	2.359	13.64	3.294	5.353	1.588	2.706	4.647
3	4.792	10.56	1.162	2.833	2.205	11.05	2.471	4.412	1.059	1.765	4.059
4	1.408	2.957	0.785	2.456	2.100	5.471	1.353	2.706	0.529	0.882	2.529
5	4.000	7.541	0.567	2.237	1.885	11.11	2.235	3.765	1.059	2.647	2.706
6	4.917	10.55	0.883	2.554	2.147	9.647	2.529	3.765	1.294	2.118	3.118
7	0.754	1.309	0.136	1.806	1.735	3.647	1.000	1.471	0.529	1.000	1.118
8	3.516	7.650	1.671	3.342	2.176	11.64	2.118	4.059	0.882	2.412	3.235
9	3.945	8.630	1.072	2.743	2.188	12.29	2.235	4.765	0.824	4.353	1.941
10	0.003	0.006	0.054	1.725	1.725	0.059	0.059	0.059	0.059	0.059	0.059

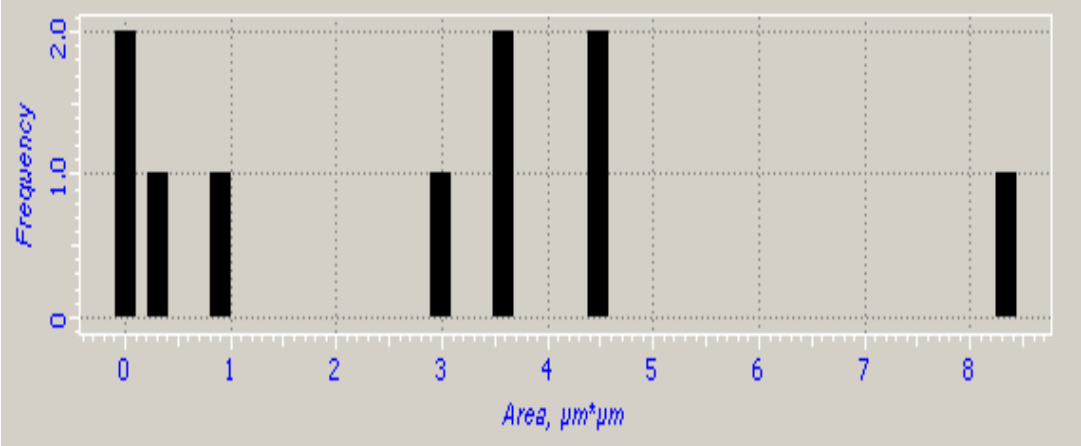

Figure 2.5 Histogram by area.

2.5 Conclusions

- Bioactive glass thin films having the composition 44.5SiO_2-11ZnO-44.5P_2O_5 (mol %). were obtained by spin-coating technique.

- For both thin film and 100ºC dried bioactive glass, the XRD results indicate an amorphous phase and nanometric crystals of zinc silicate and zinc phosphate formed during sample preparation as a consequence of residuals in the starting reagents.

- The large mass loss recorded in 203-297 ºC temperature range for the dried bioactive glass sample is related to removal of water molecules retained in cavities that suggest certain porosity, also expected for the thin films.

- AFM analysis of the thin films points out a rough, inhomogeneous surface with roughness heights around 3µm and areas up to 8.63µm^2, convenient for the attachment of biomolecule

3. *EXPERIMENTAL RESULTS OF BIOACTIVE GLASSES WITH AND WITHOUT POLYETHYLENE-GLYCOL (PEG)*

3.1 Samples synthesis

The $60SiO_2 \cdot (35\text{-}x)CaO \cdot xZnO \cdot 5P_2O_5$ glass-ceramic system, $0 \leq x \leq 10$ mol%, with four different molar ratios (Table 3.1),was prepared following the sol-gel route.

Table 3.1 Nominal composition of studied systems

Sample	SiO2(mol%)	CaO(mol%)	P2O5(mol%)	ZnO(mol%)
0%Zn	60	35	5	0
3%Zn	60	32	5	3
7%Zn	60	28	5	7
10%Zn	60	25	5	10

The precursors used were tetraethyl orthosilicate (TEOS), calcium nitrate tetrahydrate ($Ca(NO_3)_2 \cdot 4H_2O$), triethyl-phosphate (TEP) and zinc nitrate hexahydrate ($Zn(NO_3)_2 \cdot 6H_2O$). The catalyst used was HNO_3. In order to obtain samples with PEG it was repeated the previous procedure and to each sol have been added polyethylene-glycol with weight ratio TEOS: PEG = 1: 0,25.

3.2 Samples characterization by thermal analysis

Differential thermal analysis (DTA) and thermogravimetric analysis (TG) were performed on Shimadzu type derivatograph DTG-GOH in order to investigate the thermal behavior of the dried samples.

The TGA curves for all the samples prepared without PEG present more regions of weight loss (Figure 3.1). In Table 3.2 are presented the temperatures at which events occur. The first weight loss that occurs around 70 ºC coincides with an endothermic peak in DTA signal and it can be associated with the remove of free water molecules. A second weight loss with more corresponding peaks in the DTA curve can be observed until 400 ºC. Those losses can be associated with the decomposition of ammonium nitrate and the elimination of water caged in the pores. The others weight losses are observed until 700ºC that can correspond to the elimination of the organic residual elements from precursors resulted during the synthesis of samples. Should be noted that, in all the DTA signals, is observed an endothermic peak around 560°C. This peak can be associated with dehydroxylation of glasses. Sample with the highest zinc concentration gives

smallest intensity of this peak. Thermal analysis indicates that the elimination of the residual elements take place up to around 700 ºC temperatures, which can be considered as thermal treatment temperature.

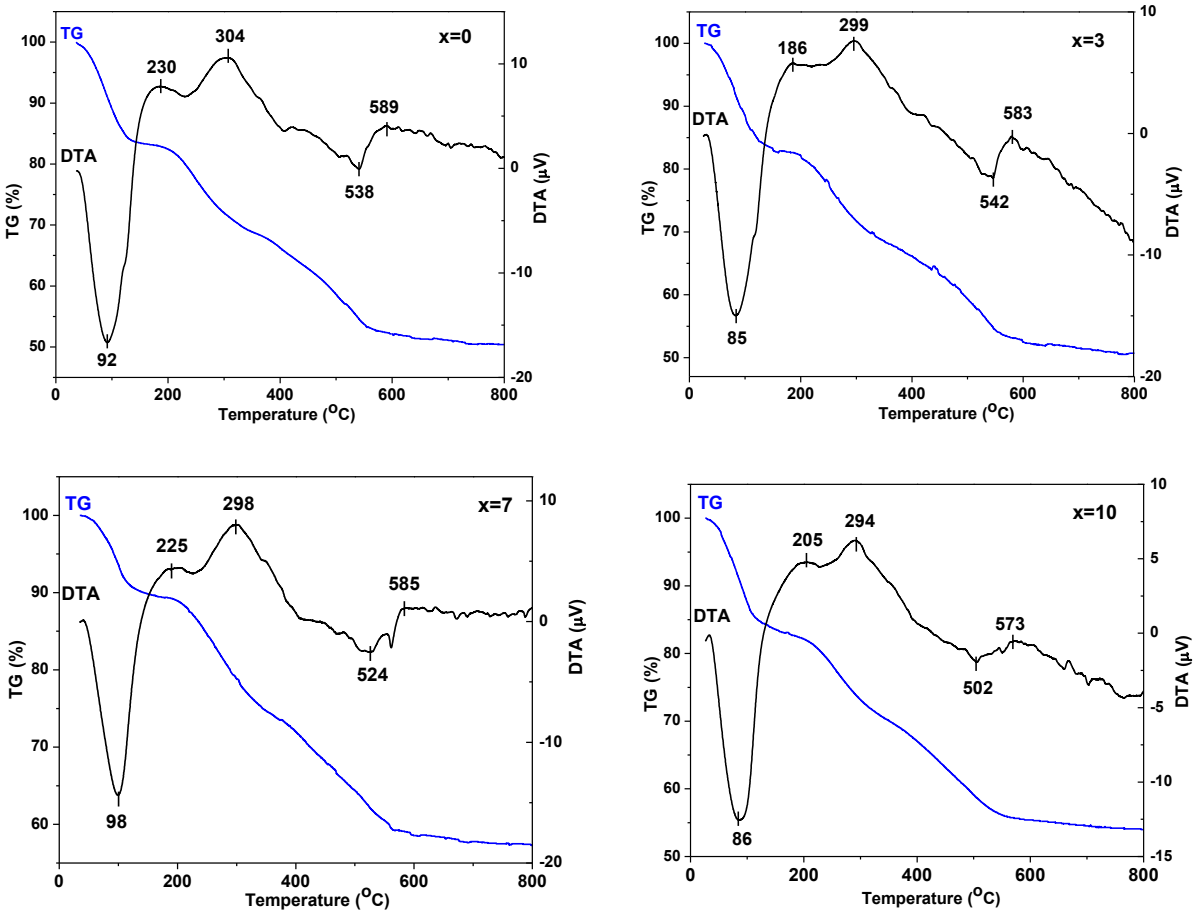

Figure 3.1 DTA and TG runs of sol-gel derived samples prepared without PEG

Table 3.2 Events temperature and weight losses for the samples prepared without PEG

Sample code	Endothermic events temperature(°C)	Exothermic events temperature (°C)	Weight losses (%)
x=0	92, 538	230, 304, 589	4.7, 18.2, 12.1
x=3	85, 542	186, 299, 583	4.2, 16.4, 11.5
x=7	98, 524	225, 298, 585	3.2, 15.7, 13.7
x=10	86, 502	205, 294, 573	4.5, 13.6, 12.8

The TGA curves for all the samples prepared with PEG present more regions of weight loss (Figure 3.2). In Table 3.3 are presented the temperatures at which events occur.

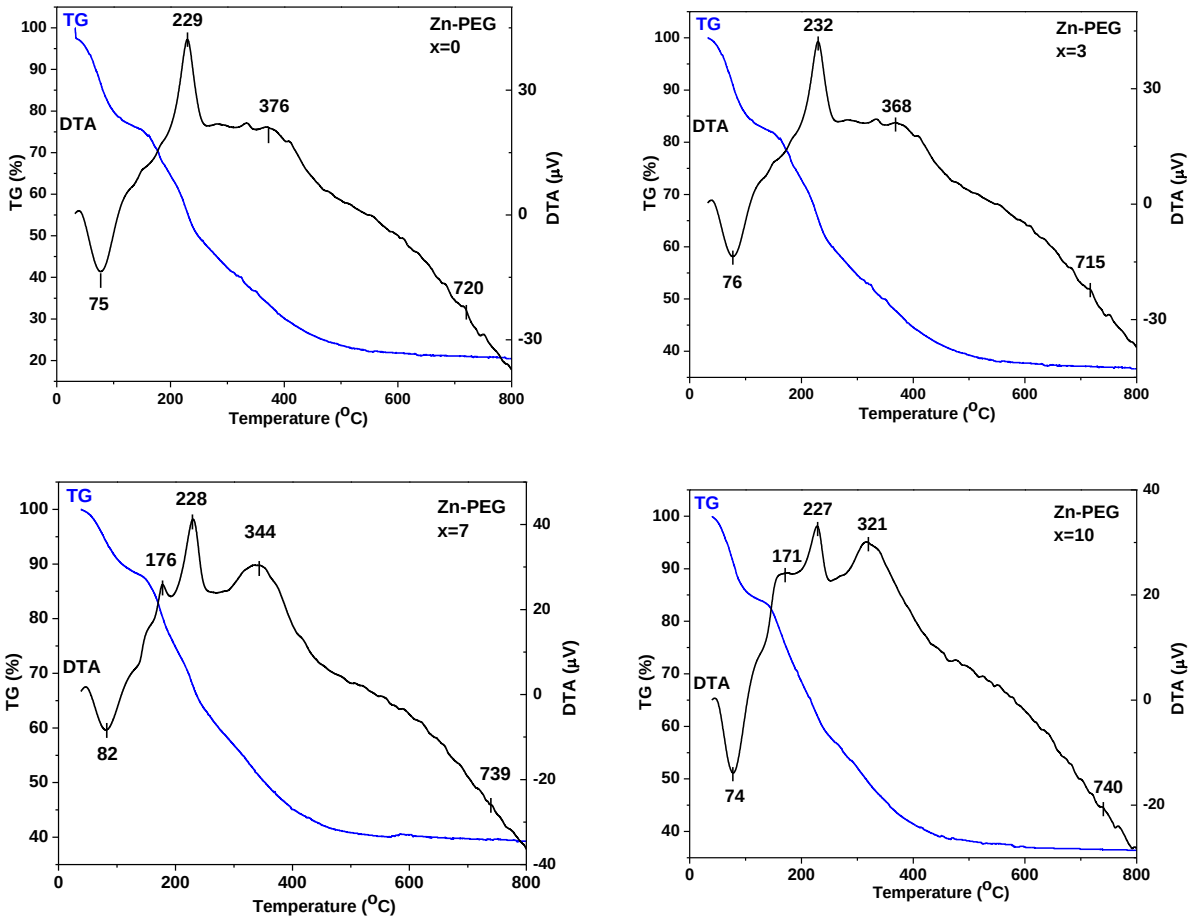

Figure 3.2 DTA and TGA runs of sol-gel derived samples prepared with PEG

Table 3.3 Events temperature and weight losses for the samples prepared with PEG

Sample code	Endothermic events temperature(°C)	Exothermic events temperature (°C)	Weight losses (%)
x=0	75	229, 376, 720	9.7, 17.2, 5.1
x=3	76	232, 368, 715	11.2, 15.6, 4.5
x=7	82	176, 228, 344, 739	8.2, 16.1, 4.7
x=10	74	171, 227, 321, 740	10.5, 14.9, 5.5

The first weight loss that occurs around 80ºC coincides with an endothermic peak in DTA signal and it can be associated with the remove of free water molecules. A second weight loss with more corresponding peaks in the DTA curve can be observed until 400ºC. Those losses can be associated with the decomposition of polyethilene-glycol and ammonium nitrate and the elimination of water caged in the pores. The others weight losses are observed until 700ºC that

can correspond to the elimination of the organic residual elements from precursors resulted during the synthesis of samples. Thermal analysis indicates that the elimination of the residual elements take place up to around 700 ºC temperatures, which can be considered as thermal treatment temperature.

3.3 Structural characterisation by X-Ray diffraction

Structure of bioglasses was characterized using X-ray diffraction (XRD) analysis with the aim to assess the crystallinity of the glasses. In the 700 ^{o}C thermal treated patterns (Figure 3.3), samples are predominately amorphous indicating the internal disorder and glassy nature of these materials.

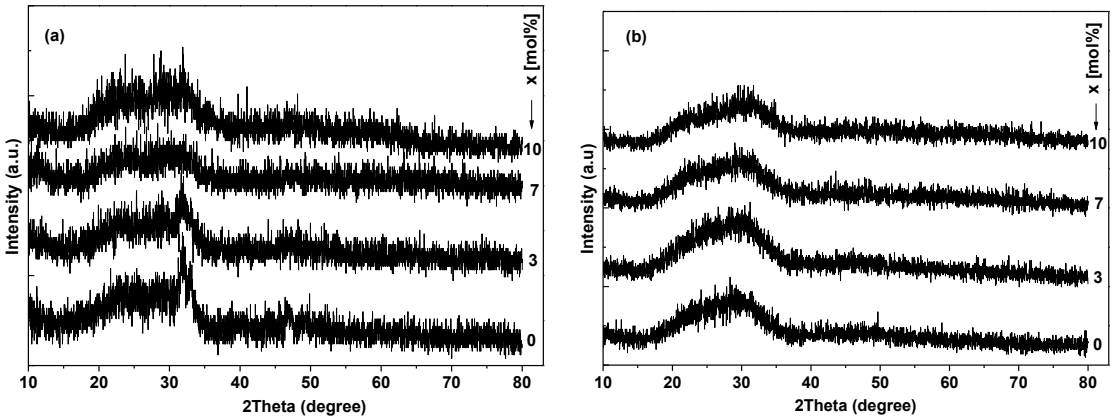

Figure 3.3 XRD patterns for samples without (a) and with (b) PEG

3.4 Structural characterisation by FTIR spectroscopy

The FT-IR spectra of the glasses prepared without PEG (Figure 3.4a) reveal the presence of a broad signal corresponding to Si-O-Si asymmetric stretching vibration in the 1000-1300cm^{-1} spectral range, which is composed of an intense absorption band centered at 1060 cm^{-1} and a shoulder around 1210 cm^{-1}. A band characteristic to Si-O-Si symmetric stretching vibration and centered at 800 cm^{-1} alongside another absorption signal assigned to Si-O-Si bending vibration and identified in the range of 500 - 400 cm^{-1} can be also seen in the recorded IR spectra [9-11]. The band observed at 945 cm^{-1} can be attributed to the Si-O stretching vibration in tetrahedral SiO_4 structure containing one non-bridging oxygen (Si-O-NBO). In the samples with 0 and 3% zinc the presence of two bands located around 570 and 605 cm^{-1} can be observed. These absorption signals are associated to P-O bending vibrations and are characteristic for crystalline apatite like phases. Their presence is in good agreement with the XRD results [12-14].

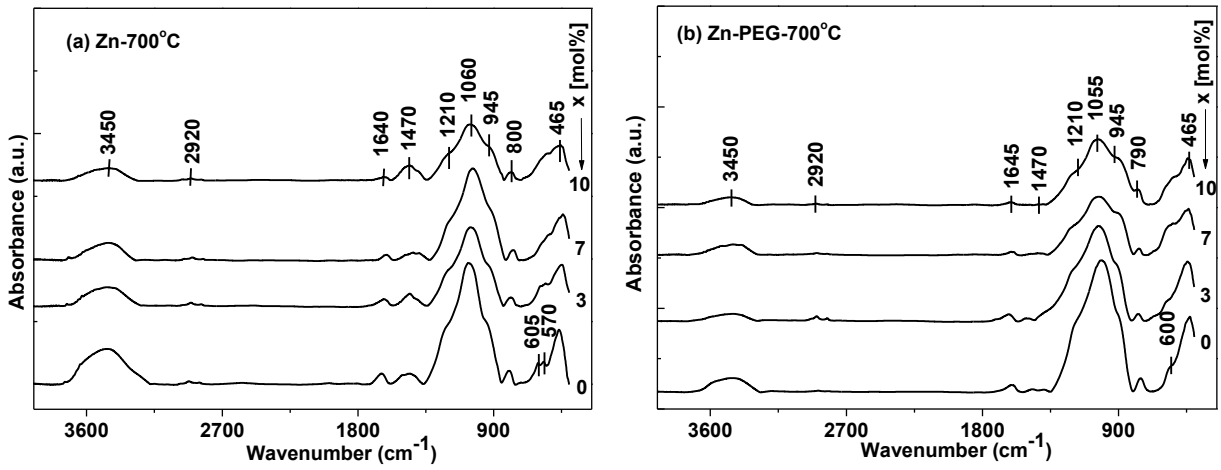

Figure 3.4 FT-IR spectra of glasses without (a) and with (b) PEG

The band seen in the range of 1560-1370 cm^{-1} is attributed to $(CO_3)^{2-}$ groups, which are present due to the carbonation of calcium containing glasses in atmospheric CO_2 [15, 16]. The band around 1640 cm^{-1} is related to molecular water [17]. The small kink situated around 2920 cm^{-1} can be associated with C-H stretching vibrations. The band observed in the range 3700-3200 cm^{-1} can be related to molecular water [18]. By progressive addition of ZnO in glasses a decrease of the IR absorption bands intensity can be observed. The FT-IR spectra of the glasses prepared with PEG (see Figure 3.4.b) reveal the same main bands as those previously discussed. By increasing the zinc content in glasses a decrease of the bands intensities can be seen.

3.5 Textural properties determinate by BET method

Figure 3.5 shows the nitrogen adsorption–desorption isotherms of the glass samples prepared without PEG and containing four different zinc compositions. The data for all samples prepared without PEG exhibit a type IV isotherm, typical of a mesoporous structure. The BET surface areas of all glass samples had some changes with the change of the chemical compositions, but all samples could reach 70–129 m^2/g as calculated from the linear part of the BET plot (Table 3.4).

Table 3.4 Specific surface area of the samples prepared without PEG

Sample	0%Zn	3%Zn	7%Zn	10%Zn

Pore specific volume (cm^3/g)	0.42	0.32	0.19	0.09
Specific surface area (m^2/g)	129.00	111.71	89.47	70.11

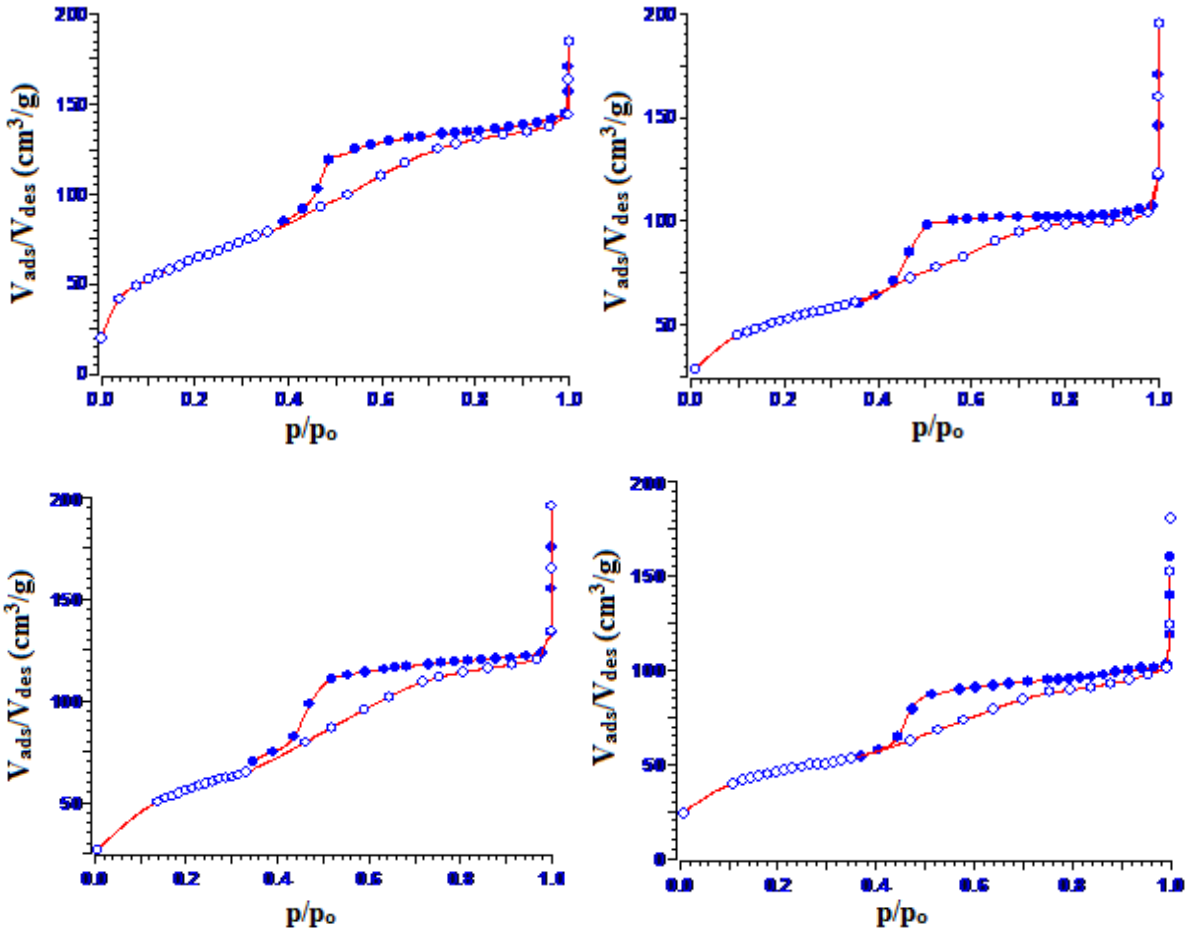

Figure 3.5 N_2 adsorption–desorption isotherms of the glass samples prepared without PEG.

The data for all samples prepared with PEG (Figure 3.6) exhibit a type IV isotherm, typical of a mesoporous structure. The BET surface areas of all glass samples had some changes with the change of the chemical compositions, but all samples could reach 112–157 m^2/g as calculated from the linear part of the BET plot (Table 3.5).

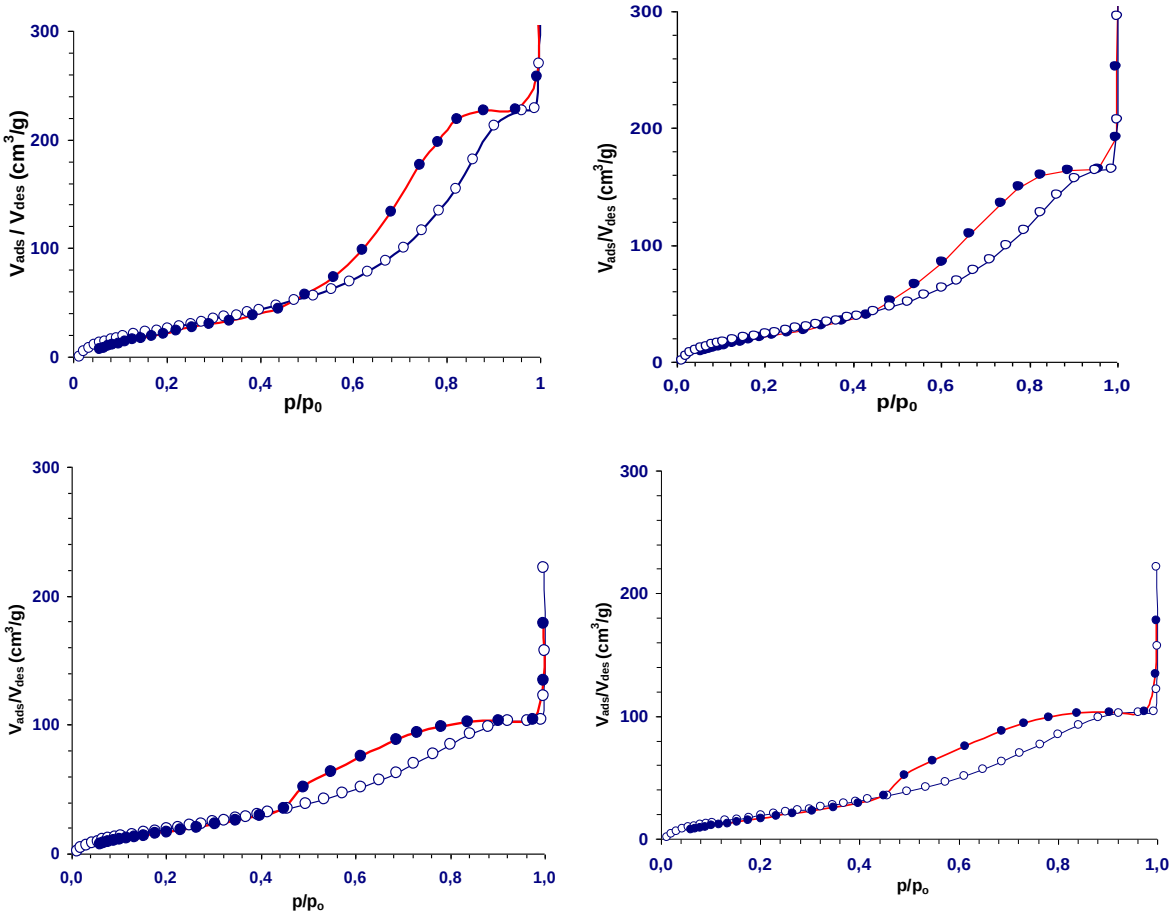

Figure 3.6 N_2 adsorption–desorption isotherms of the glass samples prepared with PEG

Table 3.5 Specific surface area of the samples prepared with PEG

Sample	0%Zn-PEG	3%Zn-PEG	7%Zn-PEG	10%Zn-PEG
Pore specific volume (cm^3/g)	0.21	0.16	0.18	0.15
Specific surface area (m^2/g)	157.00	129.71	145.47	112.11

One can conclude that both sample types present a mesoporous structure, but PEG addition during samples synthesis conferred higher specific surface areas.

3.6 Bioactivity assays

3.6.1 X-Ray diffraction

After immersion in SBF, a widen diffraction peak appears at 2θ ranging between 31° and 34° (Figure 3.7). This peak corresponding to the apatite crystallinity decreases in intensity with the increase of ZnO content.

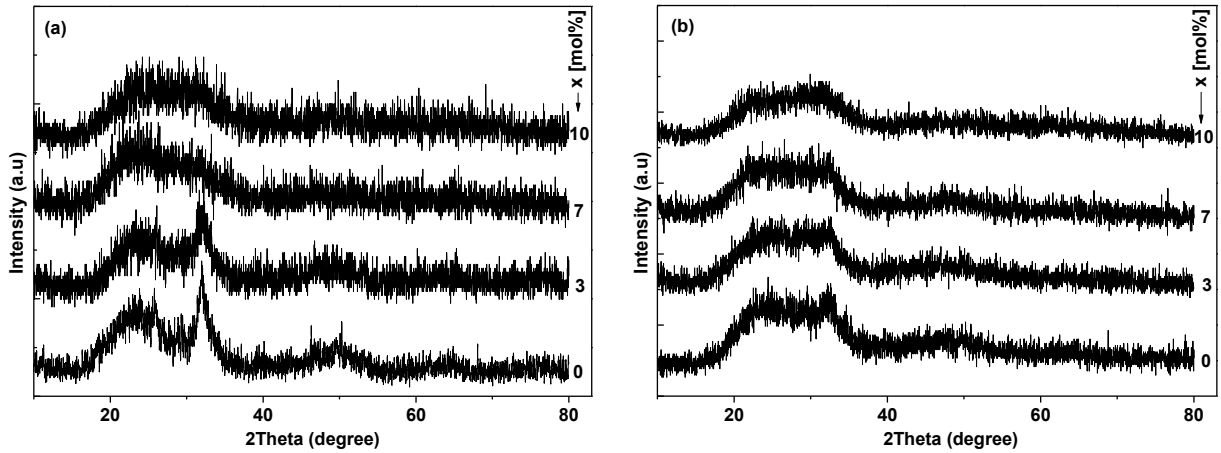

Figure 3.7 XRD patterns for samples without (a) and with (b) PEG after 14 days of SBF immersion

3.6.2 FTIR spectroscopy

After 14 days of soaking in SBF the absorption bands of the phosphate groups at 605 and 570 cm-1, together with the absorption bands of the carbonate groups at 1482, 1428, and 875 cm-1, that are in concordance with FT-IR spectra of HCA, decrease in intensity with the increase of ZnO content (Figure 3.8). One can observe that PEG addition during samples synthesis has no influence on 700 ^{O}C thermal treated samples bioactivity.

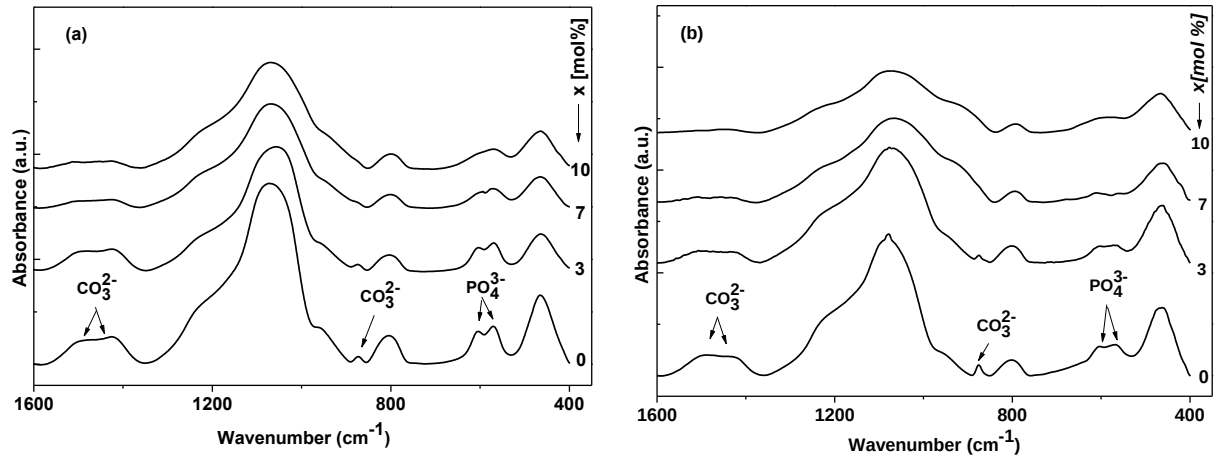

Figure 3.8 FT-IR spectra of glasses prepared without (a) and with (b) PEG after 14 days of SBF immersion

3.7 Antibacterial studies

For antibacterial tests the *Escherichia coli* cells strain XL1 blue were grown in LB media ON at 37°C. The next day, the CFU were counted (Table 3.6). For the negative control no powder was added to the bacterial culture. The obtained results (Figure 3.9) indicate that no obvious changes had place for the four different zinc concentrations comparing with the control sample. One can conclude that these zinc concentrations have no antibacterial effect and thus are suitable for cell viability tests.

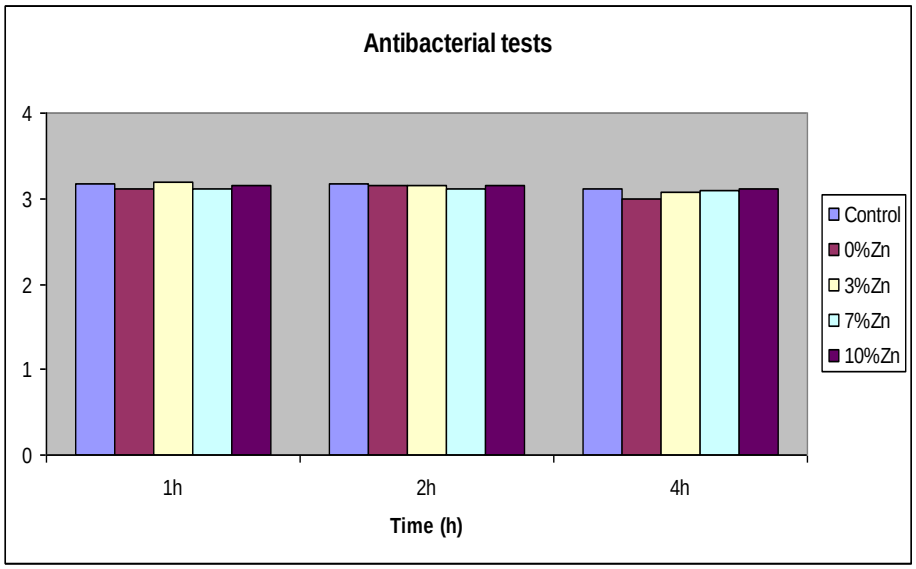

Figure 3.9 CFU as function of time

Table 3.6 CFU after incubation with glasses for different time periods.

Time (h)	Samples code				
	Control	**0%Zn**	**3%Zn**	**7%Zn**	**10%Zn**
1	3,176091	3,103804	3,192846	3,12156	3,154424
2	3,164947	3,144263	3,158362	3,107888	3,143015
4	3,113943	3,001301	3,082426	3,084576	3,120903

3.8 Samples irradiation

3.8.1 FTIR spectroscopy

Both mentioned type of samples were exposed two times to gamma rays and further investigated by means of IR spectroscopy. Each glass sample was subjected to a total dose of 386 and 1169 Gy.

The IR spectra of the glasses prepared without PEG exposed to a first dose of gamma radiation (386 Gy), show several spectral changes (Figure 3.10.a). Thus, the band situated at 1060 cm^{-1} in the IR spectrum of the zinc free glass is shifted to higher wavenumbers (1085 cm^{-1}). The shift of this absorption signal may be assumed to indicate the generation of radiation-induced defects including the changes in bond angle and/or bond lengths of Si-O-Si bonds [19]. With the progressive increase of ZnO concentration the shift of the absorption band position becomes smaller. The glasses behavior can be explained by the short range structural modifications occurred due to the presence of Zn^{2+} ions which form structural ZnO_4 groups, these units strengthening the glassy network. Also, the gamma irradiation affects the IR bands corresponding to water (1640 cm^{-1}) by shifting them to higher wavenumbers. This spectral behavior is less pronounced as the zinc concentration increases. Thus, one can conclude that the gamma irradiation of the obtained glasses caused changes not only on the main bands due to modifications occurred inside SiO_4 structural units, but on the interstitial components too. On the other side zinc addition in the glassy network conferred resistance to the samples against gamma irradiation.

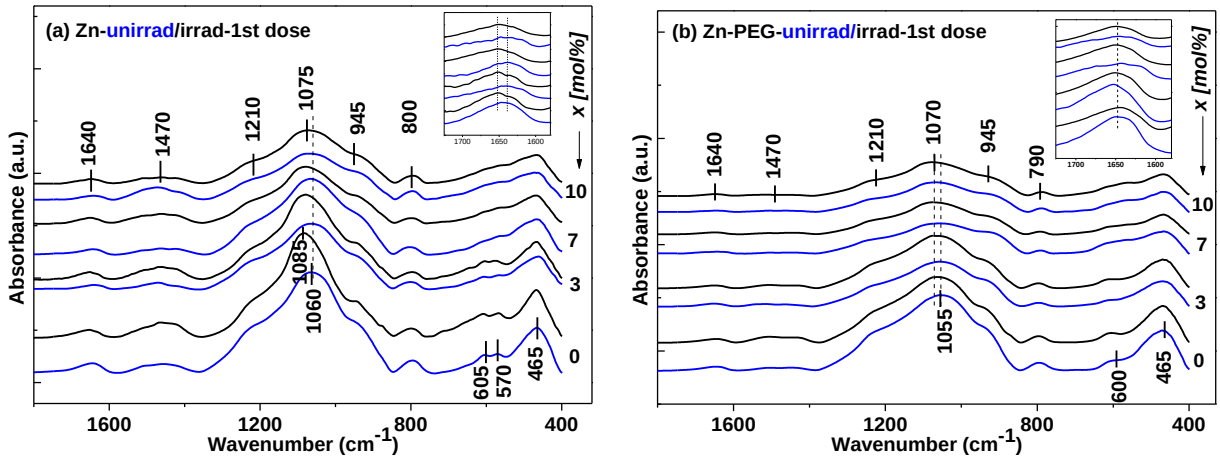

Figure 3.10 FT-IR spectra of the unirradiated and irradiated (386 Gy) sol-gel derived bioactive glasses, without (a) and with PEG (b).

In the case of samples prepared with PEG, the first dose of gamma irradiation (see Figure 3.10.b) causes some small changes of the IR band position situated at 1055 cm^{-1} and the progressive addition of ZnO seems to not influence the shift. Also, the changes in the band position corresponding to water molecules after gamma irradiation consist in a very small shift in opposite direction as in the case of glasses without PEG.

Subjecting the glass samples, prepared without PEG, for the second time to gamma irradiation with a total dose of 1169 Gy, the IR spectra reveal some obvious changes (Figure 3.11.a and b). The observed modifications suggest that the second dose of radiation has caused the breakage of the two kinds of carbonate linkages. In all the irradiated glass samples the spectra show the presence of other new bands.

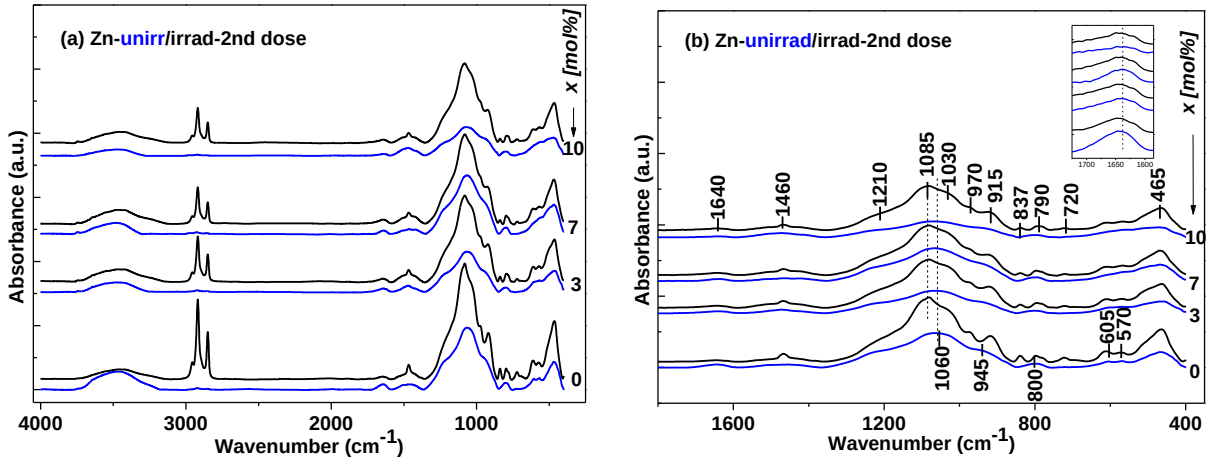

Figure 3.11 FT-IR spectra of the unirradiated and irradiated (1169 Gy) sol-gel derived bioactive glasses, prepared without PEG, in the range of 4000-400 cm^{-1} (a) and 1800-400 cm^{-1} (b).

Appearance of new bands can be explained by the facts that increasing the dose of irradiation, the silicate and phosphate network are cleaved leading to the formation of more non-bridging oxygens in the glasses. Also one can observe that by successive addition of ZnO, decrease the intensity of the new formed bands, confirming the previous assumption that zinc strengthens the glassy network.

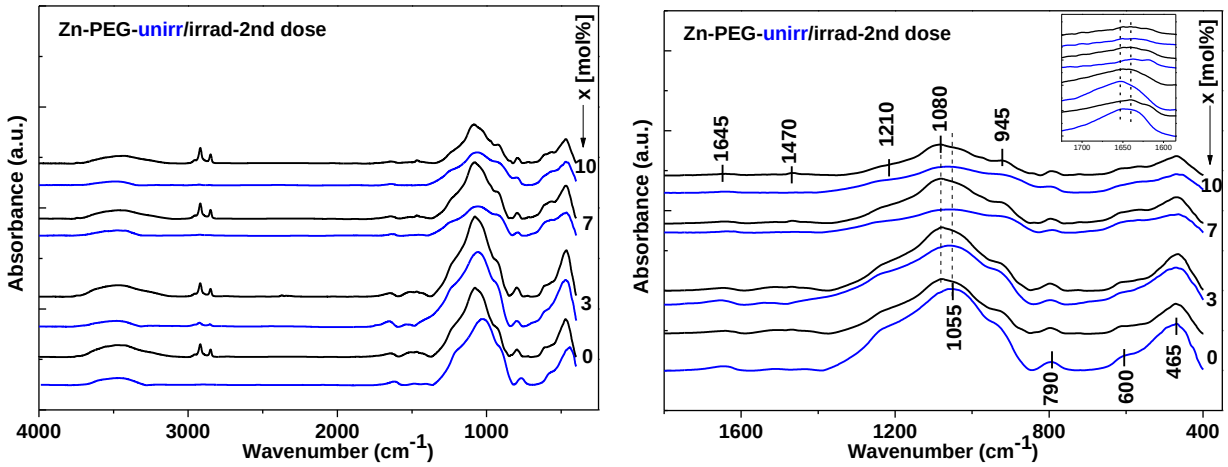

Figure 3.12 FT-IR spectra of the unirradiated and irradiated (1169 Gy) sol-gel derived bioactive glasses prepared with PEG, in the range of 4000-400 cm^{-1} (a) and 1800-400 cm^{-1} (b).

For the samples prepared with PEG, the second dose of irradiation produced not so large changes (Figures 3.12.a and b), the PEG addition during samples synthesis has conferred resistance to the glasses against irradiation, preserving thus the glass network stability.

In conclusion, by increasing the dose of irradiation, Zn^{2+} ions have lost their ability to strengthen the glass samples network. Also it is found that gamma irradiation effect in the case of glasses prepared with PEG is much lower than for the glasses prepared without PEG.

3.8.2 UV-visible spectroscopy

The UV–visible absorption spectra of the glasses prepared without PEG, before and after the first dose of irradiation, are illustrated in Figure 3.13.a. Before the first dose of irradiation, the undoped glass spectrum reveals a strong UV absorption band centered at about 215 nm and a curvature, which is starting around 360 nm, from which the absorption level of the sample is considerably increased. After ZnO addition, the UV signal observed at higher energies in the undoped sample starts to decrease in intensity and is becoming just a kink for the highest zinc concentration. The absorption band located around 360 nm becomes more defined as the zinc content increases, but in the meantime, the absorption signal recorded in the visible spectral domain, *i.e. 400-600 nm*, is progressively decreasing in intensity

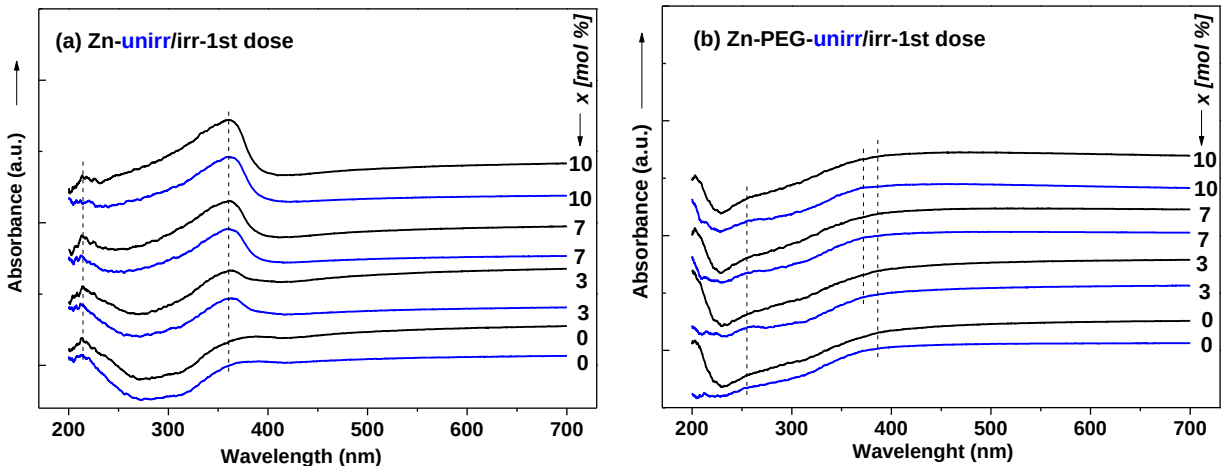

Figure 3.13 UV-visible spectra for glassy samples prepared without (a) and with PEG (b), before and after gamma irradiation (386 Gy).

The first dose of gamma irradiation had effect just on iron ions, the amount of non-bridging oxygens formed by zinc introduction in the glass matrix remaining unaffected.

UV–visible absorption spectra of the samples prepared with PEG, before and after the first dose of gamma ray irradiation, are illustrated in Figure 3.13.b. In the case of the samples

before irradiation, the undoped glass reveals a small UV absorption band centered at about 214 nm, a shoulder around 260 nm and a curvature at 385 nm. After ZnO addition, the UV small band observed at 214 nm in the undoped sample starts to modify and for the highest zinc concentration becomes a shoulder. The shoulder located around 260 nm becomes more pronounced as zinc content is higher. The curvature situated around 385 nm in the undoped sample is slightly shifted to smallest wavelengths after the zinc addition and the absorption signal recorded on the visible spectral domain is decreasing in intensity.

On subjecting these glasses to a total gamma dose of 386 Gy, the UV spectrum for the undoped sample reveals a sharp absorption peak at about 200 nm, two shoulders around 225 nm and 260 nm and a curvature at about 395 nm. On the addition of ZnO, the UV sharp band observed in the undoped sample at about 200 nm seems to change its intensity with the increase of zinc amount. In fact, these modifications of the band shape are caused by the progressive increased absorption of the signal recorded between 200 and 210 nm with the zinc addition. The shoulder situated at about 225 nm decreases in intensity, whereas the shoulder located at 260 nm becomes better defined. The curvature centered on 395 nm in the undoped sample seems to be shifted to smaller wavelenghts by the increasing of the zinc content. The spectrum of the irradiated samples reveals no significant changes in the visible spectral domain, where the absorption signal is significant.

The analysis of the absorption recorded on the UV and visible domains, before and after irradiation, shows a clearly different behavior, as zinc content increases, for the two series of samples. As mentioned, for the samples before irradiation, the UV signal increases in intensity and the visible one decrease with the addition of zinc, while after irradiation, the UV signal slowly decreases and the visible one is almost constant.

After the second dose of irradiation (Figure 3.14.a), the samples prepared without and with PEG show absorption bands attributed to the presence of trace iron impurities due to unavoidable contamination alongside to absorption spectra that correspond to the formation of non-bridging oxygens due to the presence of network modifiers, especially to zinc. The progressive addition of zinc in the two kinds of samples produces different effects on the formation of the UV absorption bands. For the samples prepared without PEG, an increase in intensity of the UV bands takes place whereas for the samples prepared with PEG the modification consists in the shift of the bands with the increase of zinc content. Also it is found that gamma irradiation in the case of glasses prepared without PEG produced a broadening of the bands, while for the glasses prepared with PEG the effect was the shift of the bands. On can

conclude that the PEG addition during samples synthesis has conferred resistance to the glasses against irradiation, preserving thus the glass network stability, results that confirm those obtained from FTIR analysis.

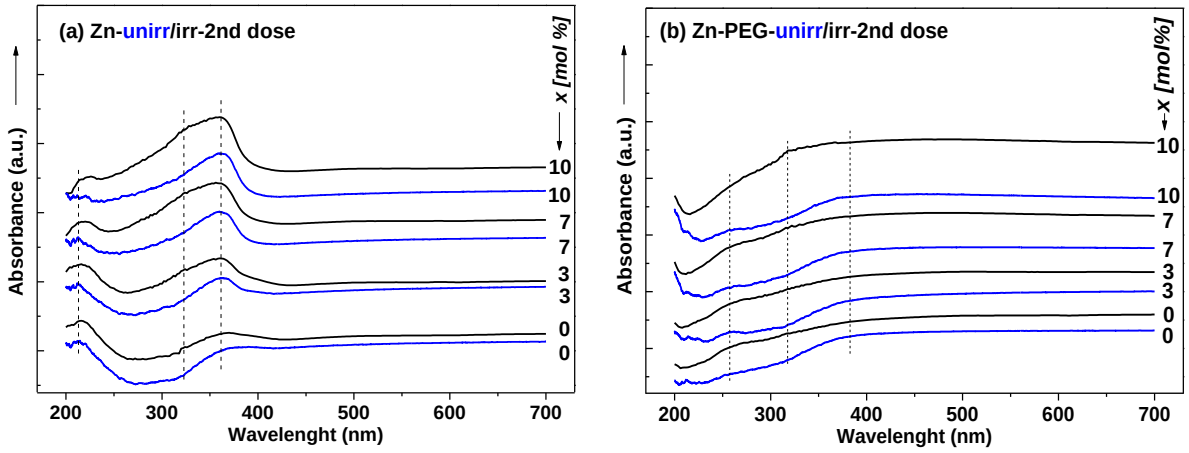

Figure 3.14 UV-visible spectra for glassy samples prepared without (a) and with PEG (b), before and after gamma irradiation (1169 Gy).

3.9 Conclusions

- Sol-gel derived samples based on ZnO-CaO-P_2O_5-SiO_2 thermally treated at 700°C have a prevailing amorphous structure indicating an internal disorder and glassy nature of these compounds.

- Both PEG added and PEG-free samples have a mesoporous structure, but PEG addition conferred highest specific surface areas and porosity.

- Samples bioactivity decreases with the increase of zinc concentration and have no antibacterial effect, which demonstrates, that the glasses with the four zinc concentrations (0, 3, 7 and 10% mol) are suitable for cell viability tests.

- Moreover zinc addition in the glassy network induces samples resistance against gamma irradiation, whereas for the increased irradiation dose, Zn^{2+} ions have lost their ability to strengthen the glass samples network.

- On the other hand PEG addition during samples synthesis confers very good resistance to the glasses against irradiation, preserving thus the glass network stability.

4. EXPERIMENTAL RESULTS OF THREE-DIMENSIONAL MACROPOROUS SCAFFOLDS

4.1 Scaffolds preparation

The $60SiO_2 \cdot (35\text{-}x)CaO \cdot xZnO \cdot 5P_2O_5$ with x = 0, 3, 7, 10 mol% glass-ceramic system was prepared following the sol-gel route. The precursors used were tetraethyl orthosilicate (TEOS), $(Ca(NO_3)_2 \cdot 4H_2O)$, triethyl-phosphate (TEP) and $(Zn(NO_3)_2 \cdot 6H_2O)$. The catalyst used was HNO_3. PEG with molecular weight 200, from Alfa Aesar, was added to the obtained sol. The polyurethane (PU) sponges, characterized by a 3-D network of macropores were immersed in the resulting sols, and then they were taken out, squeezed and left to dry on a smooth surface for 24 hours at room temperature. The process was repeated for five times and followed by a heat treatment for burning out of the polymer template and sintering of the final scaffold (see Figure 4.1).

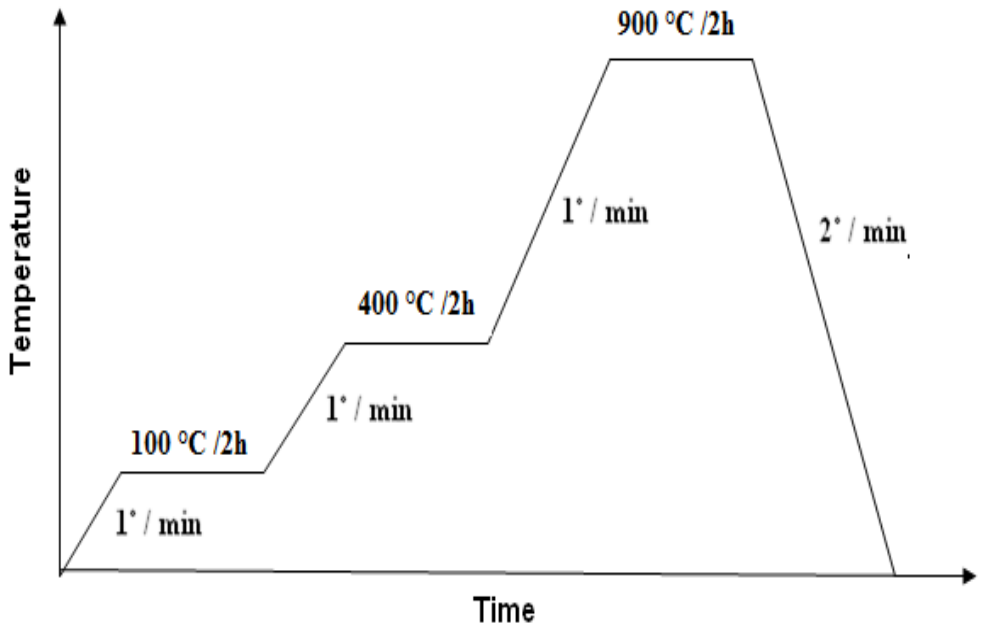

Figure 4.1 Heat treatment schedule to achieve the final scaffolds

4.2 Samples characterization by thermal analysis

Differential thermal analysis (DTA) and thermogravimetric analysis (TG) were performed in order to investigate the thermal behaviour of the 100 ^{o}C dried scaffolds, and to assess the heat treatment temperatures in order to obtain the final scaffolds.

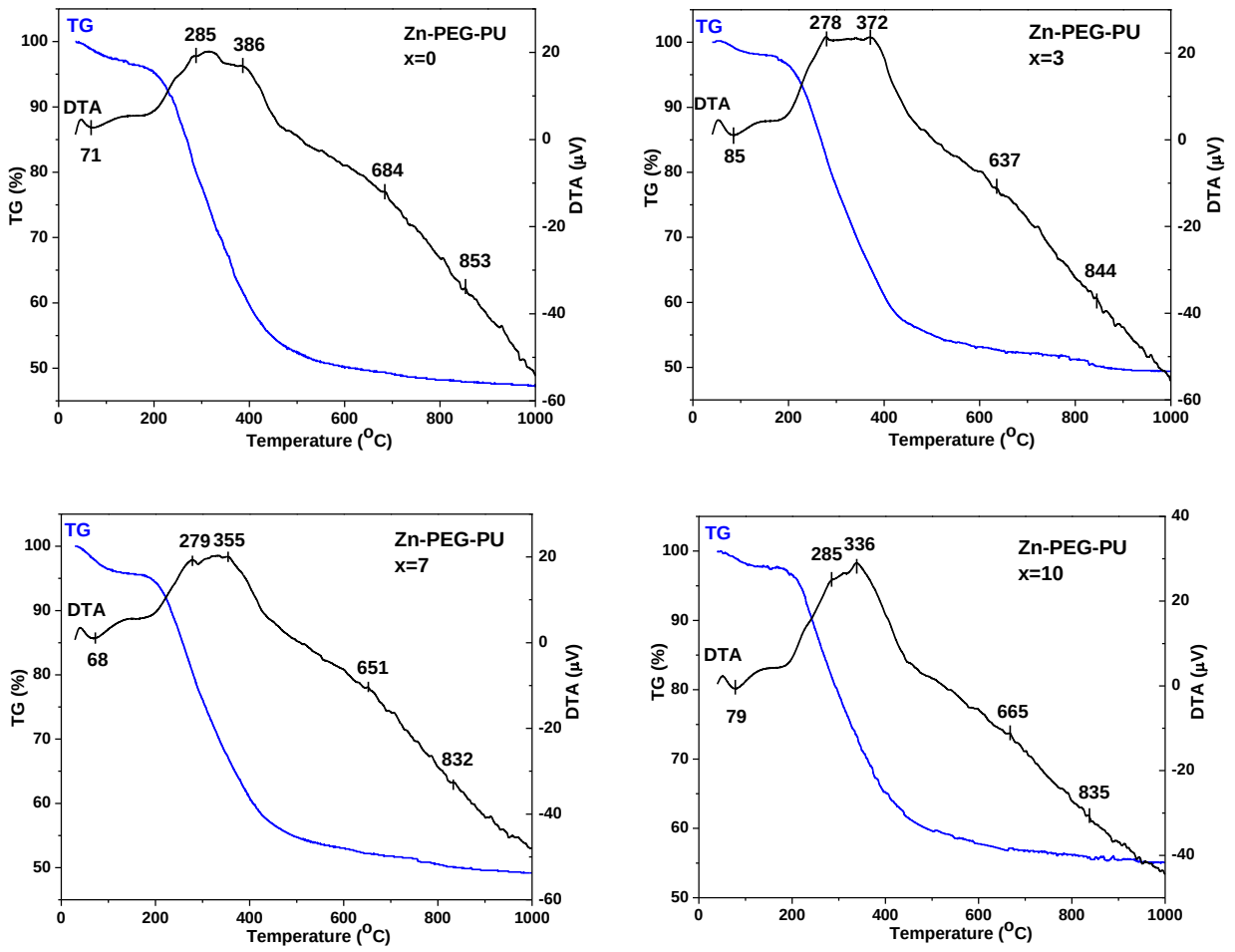

Figure 4.2 DTA and TG runs of the obtained scaffolds with added PEG (Zn-PEG-PU)

Table 4.1 Events temperature and weight losses for the scaffolds prepared with PEG

Sample code	Endothermic events temperature(°C)	Exothermic events temperature (°C)	Weight losses (%)
Zn-PEG-PU, x=0	71, 684	285, 386, 853	3.5, 45.7, 3.1
Zn-PEG-PU, x=3	85, 637	278, 372, 844	2.2, 41.1, 6.9
Zn-PEG-PU, x=7	68, 651	279, 355, 832	4.1, 38.9, 7.4
Zn-PEG-PU, x=10	79, 665	285, 336, 835	1.9, 37.9, 4.6

The TG curves for the samples prepared with PEG present more regions of weight loss (Figure 4.2). In Table 4.1 are presented the temperatures at which events occur. The first weight loss that occurs around 65-85 ºC coincides with an endothermic peak in DTA signal and it can be associated with the removal of free water molecules. A second weight loss with more

corresponding peaks in the DTA curve can be observed until 400 ºC. This loss can be associated with the decomposition of polyurethane and polyethilene-glycol and the elimination of water caged in the pores. Further weight losses are observed until 800 ºC and correspond to the elimination of the organic residual groups from the precursors used in the samples synthesis. Thermal analysis also indicates that the sol-gel glass crystallization temperature occurs in the range of 830-860 ºC through an exotermic peak revealed by differential thermal calorimetry (DTA). Glass-ceramic scaffolds can be obtained until 900 ºC, which can be considered as thermal treatment temperature.

The TG curves for the samples prepared without PEG present more regions of weight loss (Figure 4.3). In Table 4.2 are presented the temperatures at which events occur.

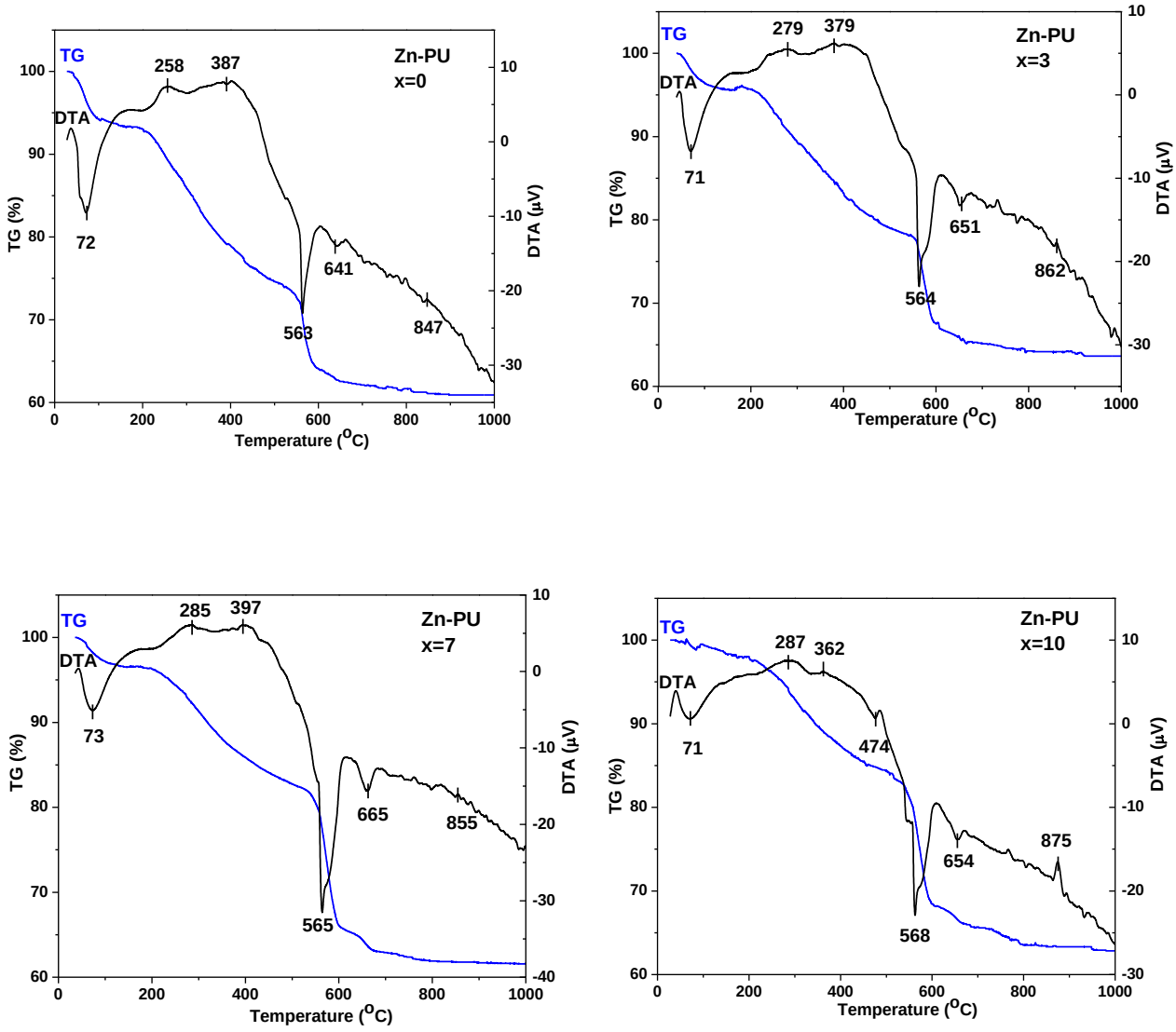

Figure 4.3 DTA and TGA runs of the obtained scaffolds without PEG (Zn-PU).

Table 4.2 Events temperature and weight losses for the scaffolds prepared without PEG

Sample code	Endothermic events temperature(°C)	Exothermic events temperature (°C)	Weight losses (%)
Zn-PU, x=0	72, 563, 641	258, 387, 847	5.7, 20.1, 10.1, 1.9
Zn-PU, x=3	71, 564, 651	279, 379, 862	3.8, 17.5, 12.3, 2.4
Zn-PU, x=7	73, 565, 665	285, 397, 855	3.5, 14.2, 16.8, 3.7
Zn-PU, x=10	71, 474, 568, 654,	287, 362, 875	4.6, 11.4, 14.9, 4.5

The first weight loss occurs around 70-75 ºC and corresponds with an endothermic peak in DTA signal and it can be associated with the removal of free water molecules. A second weight loss wich coincides with two exotermic peaks in the DTA curve can be observed until 400 ºC. This loss can be associated with the decomposition of polyurethane and the elimination of water caged in the pores. Further weight losses are observed until 800 ºC and correspond to the dehydroxilation process in the rage of 560-570 ºC and the elimination of the organic residual groups from the precursors used in the samples synthesis. Thermal analysis also indicates that the sol-gel glass crystallization temperature occurs in the range of 860-885 ºC through an exotermic peak revealed by differential thermal calorimetry (DTA). The proper temperature that can be used for thermal treatment in order to obtain glassy samples it seems to be 700 ºC. Also glass-ceramic scaffolds can be already obtained until 900 ºC, which can be considered as sinthering temperature in order to obtain the finnal scaffolds.

4.3 Structural characterisation by X-Ray diffraction

The structural changes that occur after the thermal treatment and sintering of the obtained samples were investigated using X-ray diffraction technique (Figure 4.4 and 4.5). X-ray diffraction patterns reveal that the 100^{o}C dried samples prepared with PEG (Figure 4.4.A) have an amorphous structure depicted by the broad diffraction peak situated between $2\theta = 20^{o}$ and 30^{o}. For the samples prepared without PEG, beside the large diffraction peak that dominates the XRD pattern, there are peaks indicating the presence of a minor crystalline structure, that could be assigned to residual ammonium nitrate crystals (NH_4NO_3) [41]

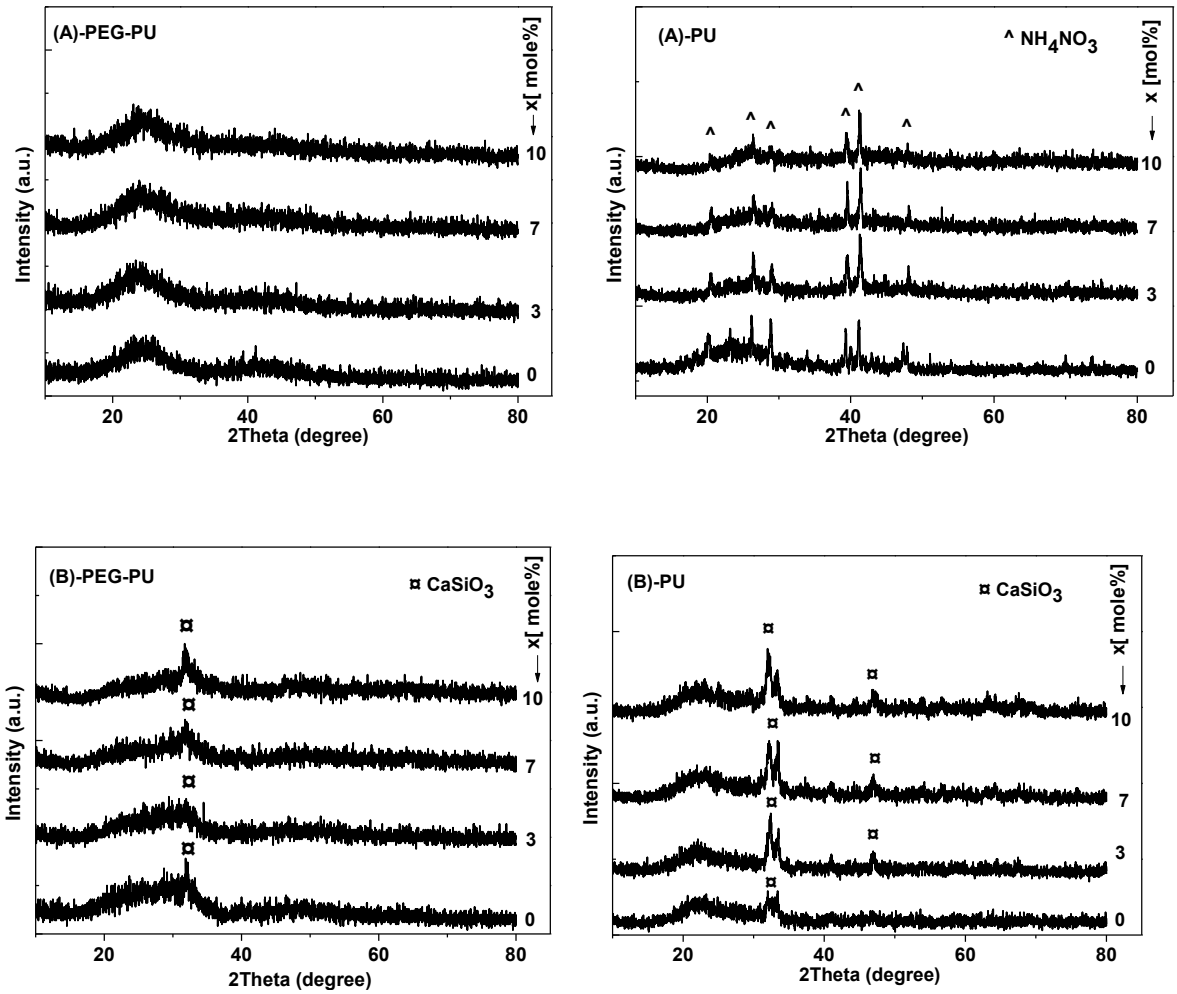

Figure 4.4 XRD patterns for 100°C dried samples (A) and 700°C heat treated samples (B) prepared with and without PEG

The 700°C thermally treated samples (see Figure 4.4.B) prepared with and without PEG are also predominantly amorphous, developing a crystalline phase that corresponds to calcium silicate ($CaSiO_3$).

XRD patterns (Figure 4.5) show the development of several nanocrystalline phases in the 900°C sintered samples. Hardystonite ($Ca_2ZnSi_2O_7$,), hydroxyapatite, pseudowollastonite ($Ca_3Si_3O_9$), wollastonite (β-$CaSiO_3$) and low cristobalite (SiO_2) were identified in the samples prepared with PEG (Figure 4.32A). As expected, the zinc-free sample doesn't presents hardystonite crystals. In the PEG-free scaffolds the nucleated phases are hardystonite, alpha-TCP [$Ca_3(PO_4)_2$], hydroxyapatite, pseudowollastonite ($Ca_3Si_3O_9$), wollastonite, low cristobalite, but hydroxylapatite diffraction peaks occur only for the sample with 0 and 3% zinc content (Fig. 4.32B). With increasing of the zinc content, the samples prepared with PEG present an increase of the intensity of hardystonite and low cristobalite peaks with the simultaneous decline of

wollastonite. Hydroxylapatite phase is well developed also, in all samples prepared with PEG whereas in the PEG-free samples it can be seen just for the 0 and 3% zinc content. The PEG–free samples present peaks that correspond to alpha-TCP phase whose intensity is less pronounced as the ZnO concentration increases from 0 to 10 mol%. The results indicate that the addition of PEG may favor the nucleation of pseudowollastonite and hydroxylapatite.

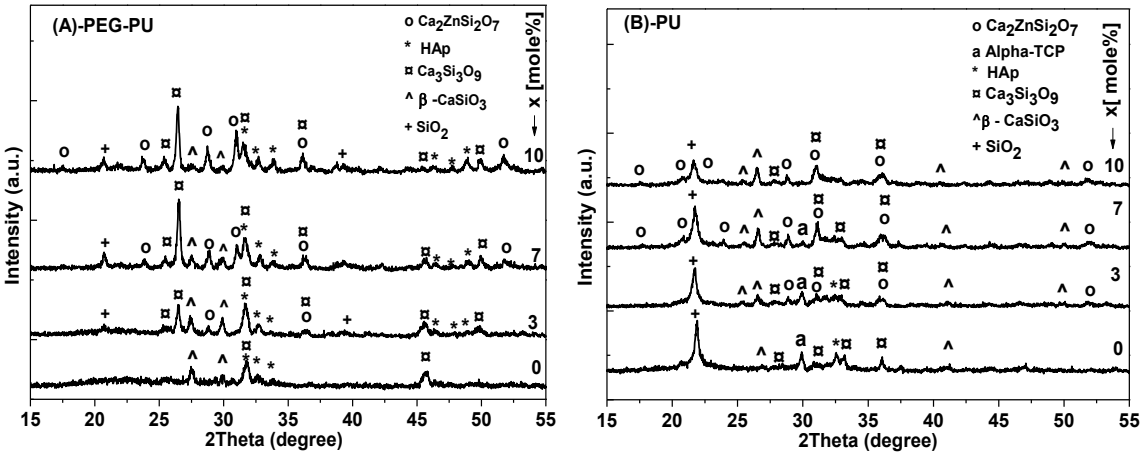

Figure 4.5 XRD patterns for sintered samples with (A) and without (B) added PEG

The pseudowollastonite crystallites size, calculated with the Scherrer equation for the samples prepared with and without PEG (Table 4.3) increase with the increase of Zn content. The samples prepared with PEG present a more uniform distribution of the crystallite size which is larger than those obtained without PEG.

Table 4.3 The size of pseudowollastonite crystallites in the samples obtained with sacrificial PU template coated with sol-gel derived glasses prepared by adding PEG and without PEG.

Sample code	Crystallite size (nm)
0%ZnO-PEG-PU	32.1
3%ZnO-PEG-PU	32.7
7%ZnO-PEG-PU	33.4
10%ZnO-PEG-PU	34.2
0%ZnO-PU	18.6
3%ZnO-PU	20.5
7%ZnO-PU	25.1
10%ZnO-PU	28.3

4.4 Structural characterisation by FTIR spectroscopy

The FT-IR spectra of the sample prepared with PEG (Figure 4.6.A) show that by progressive addition of ZnO, takes place the appearance of new bands. The intensity of the bands associated to the vibration of Si-O-NBO and Si-O-2NBO groups increases with zinc concentration indicating that the vitreous silica network suffers a net decrease in its local symmetry due to the zinc addition. The band observed still at 940 cm^{-1} for 3% zinc content is shifted to 970 cm^{-1} simultaneously with the increase of the zinc concentration. This means that Zn^{2+} ions tend to act as a network modifier in a stronger fashion than the Ca^{2+} ions [20]. Despite the fact that ZnO has the ability to play both the role of network modifier and of intermediate oxide, in the investigated samples zinc ions act only as glass network modifier.

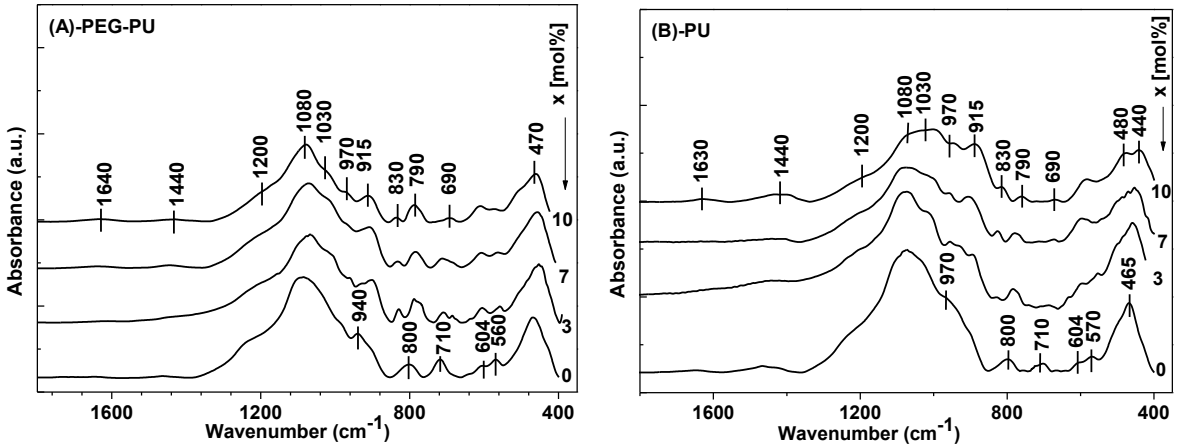

Figure 4.6 FT-IR spectra of the obtained scaffolds with (A-PEG-PU) and without (B-PU) added PEG

The band situated around 710 cm^{-1} due to asymmetric P-O-P stretching vibration [21, 22], exhibit a progressive reduction in the relative intensity and a slight shift to lower wavenumbers with increasing the zinc concentration. This behavior can be explained by the change in the chain P-O-P bond angles as an effect of the modifiers on the network structure [23]. The presence of two well resolved bands around 570 and 604 cm^{-1} can be observed in all the samples prepared with PEG. These bands are assigned to P-O bending vibration in PO_4^{-3} tetrahedra characteristic for crystalline apatite like phases [24-26], and are in good agreement with the XRD results.

In comparison with the spectra recorded from samples prepared with PEG, for that prepared without PEG (see Figure 4.6.B) it was observed that the characteristic absorption band related to Si-O-Si stretching vibration (1080 cm^{-1}) is broader whereas the intensity of the bands corresponding to Si–O–Si bending vibration (400-500 cm^{-1} and 800 cm^{-1}) is sharper. Also, the bands corresponding to Si-O-NBO and Si-O-2NBO bonds are better evidenced in the PEG-free

samples, for which the degree of network connectivity decreases by replacement of silicon bridging oxygen bonds with silicon non-bridging oxygen bonds [27]. In the case of the samples prepared without PEG, the two bands close to 600 cm^{-1}, assigned to P-O bending vibration typical for hydroxyapatite phase, are recoded only from the sample without and with the lowest zinc content, x = 0 and 3% ZnO. On the other side, the polymer introducing during the samples synthesis provided a thermodynamically favorable environment for further development of hydroxyapatite crystalline phase.

4.5 Scanning Electron Microscopy

SEM images (Figure 4.7.A and B) of the obtained scaffolds can be used for the study of macropores size and interconnectivity as well as samples microstructure. Glass-ceramic scaffolds produced by sacrificial template method maintained the pore interconnectivity of its polyurethane spongy template. The PEG addition during samples synthesis did not modified the macropores dimension, SEM images revealing the macroporous morphology of all the sintered scaffolds with a pore diameter of 300-500 μm. Also, for both types of samples, the microstructure is dependent of the glass-ceramics chemical composition which results in a relatively denser texture for the highest concentration of zinc. Based on SEM images, one can conclude that glass-ceramic scaffolds prepared by PEG addition maintain a better interconnectivity and a relatively different microstructure.

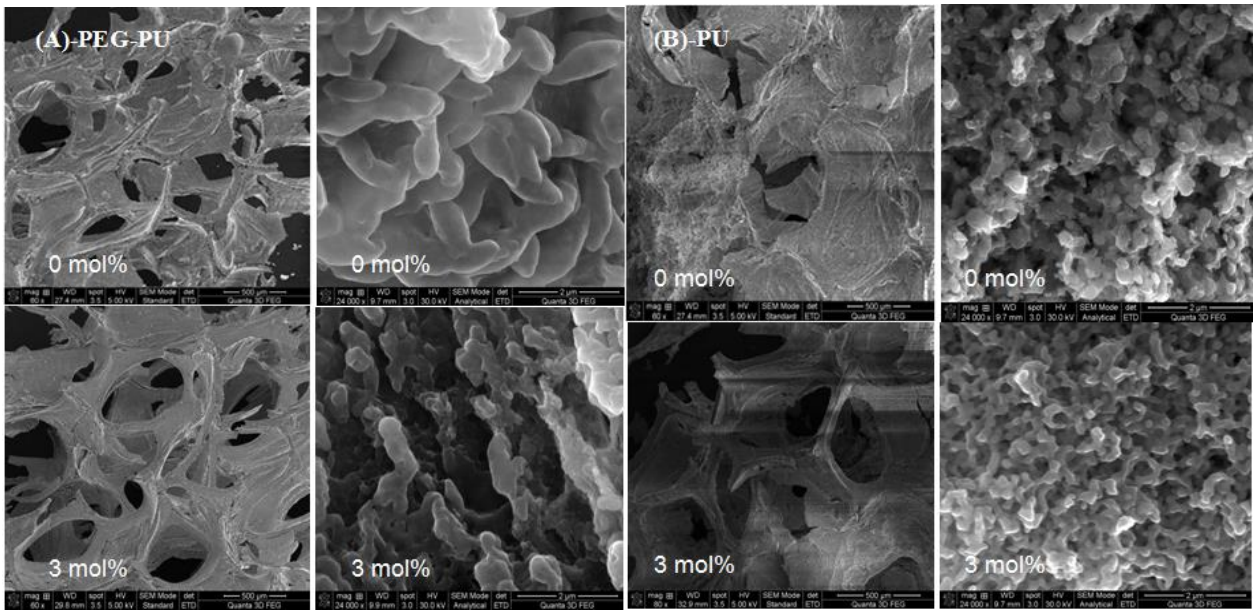

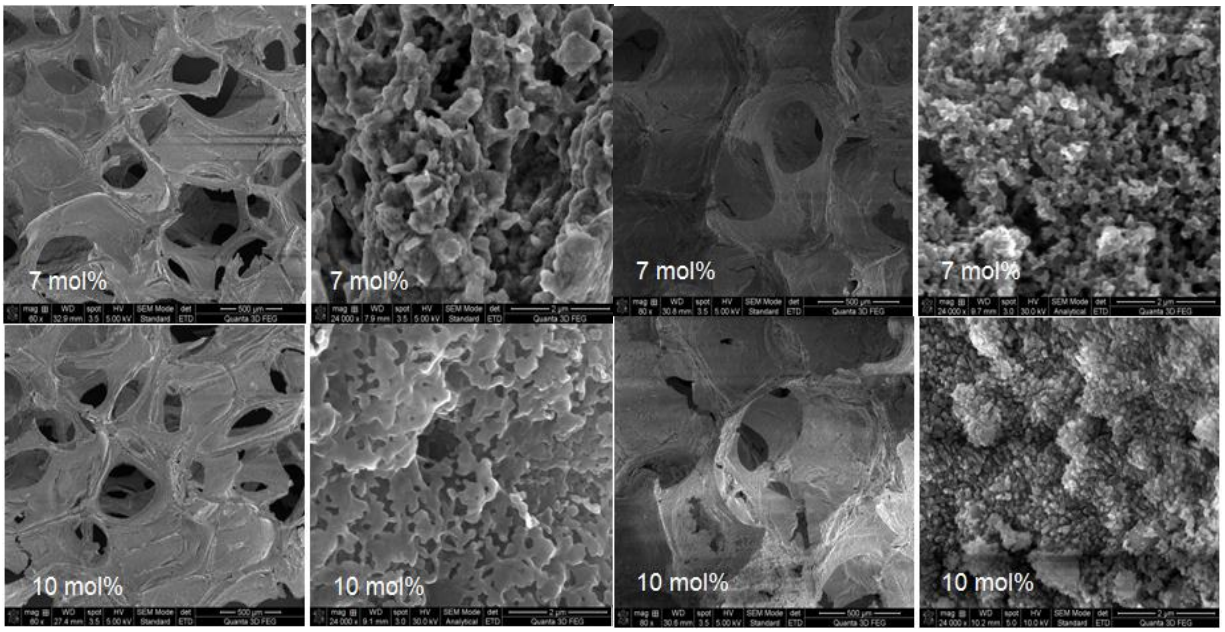

Figure 4.7 Pore structure and microstructure for the samples obtained with (A-PEG-PU) and without (B-PU) PEG.

4.6 Bioactivity assays

4.6.1 X-Ray diffraction

Assessment of bioactivity was carried out on glass-ceramic samples after 14 days of immersion in SBF using XRD, FT-IR and SEM. The XRD patterns of the samples prepared with PEG recorded before and after their immersion in SBF (Figure 4.8.A, B, C and D), reveal that the hydroxyapatite phase occur in all these samples even before SBF immersion, and is better developed with the increase of zinc concentration. In the PEG–free samples, before immersion,

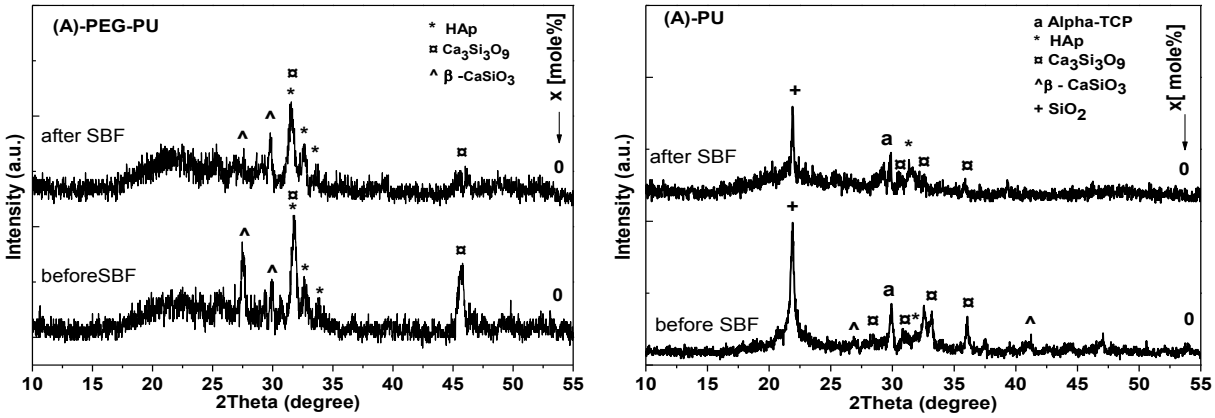

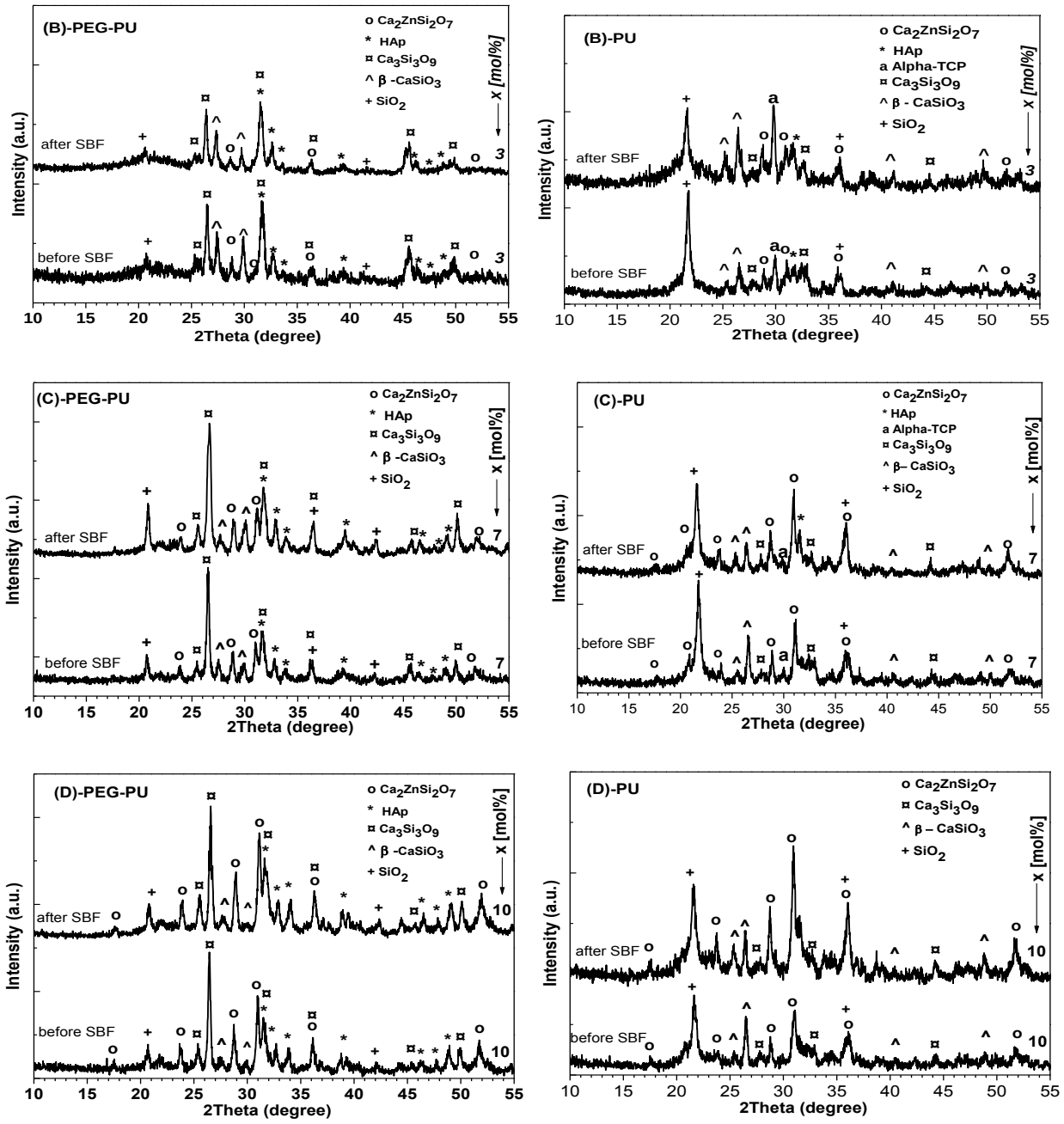

Figure 4.8 XRD patterns for the PEG containing and PEG –free sample with 0% ZnO (A), 3% ZnO (B), 7% ZnO (C) and 10% ZnO (D), before and after 14 days of immersion in SBF.

the presence of hydroxylapatite phase was observed just for the zinc-free sample and the lowest zinc content whereas in the immersed scaffolds was present for 0, 3 and 7% ZnO (Figure 4.8).

Scaffolds soaked in SBF showed an inhibitory effect on the apatite formation in case of the PEG–free prepared sample with highest zinc content. Obviously, the polymer addition during samples synthesis was beneficial for their bioactivity regardless of the zinc concentration.

4.6.2 FTIR spectroscopy

The XRD results are confirmed by FT-IR analysis performed on the glass-ceramic samples after 14 days of immersion in SBF. FT-IR spectra of the samples prepared without PEG reveal no new band after 14 days of immersion in SBF (Fig. 4.9.A, B, C and D). These spectroscopic results prove that the local structure of the samples cannot be destroyed by SBF ions migration into glass surface. The double band located at 570 and 604 cm^{-1} corresponding to the P–O bending vibrations and characteristic to the crystalline hydroxyapatite phase [71-73] is present in the spectra of samples with $x \leq 7$ mol % ZnO immersed in SBF.

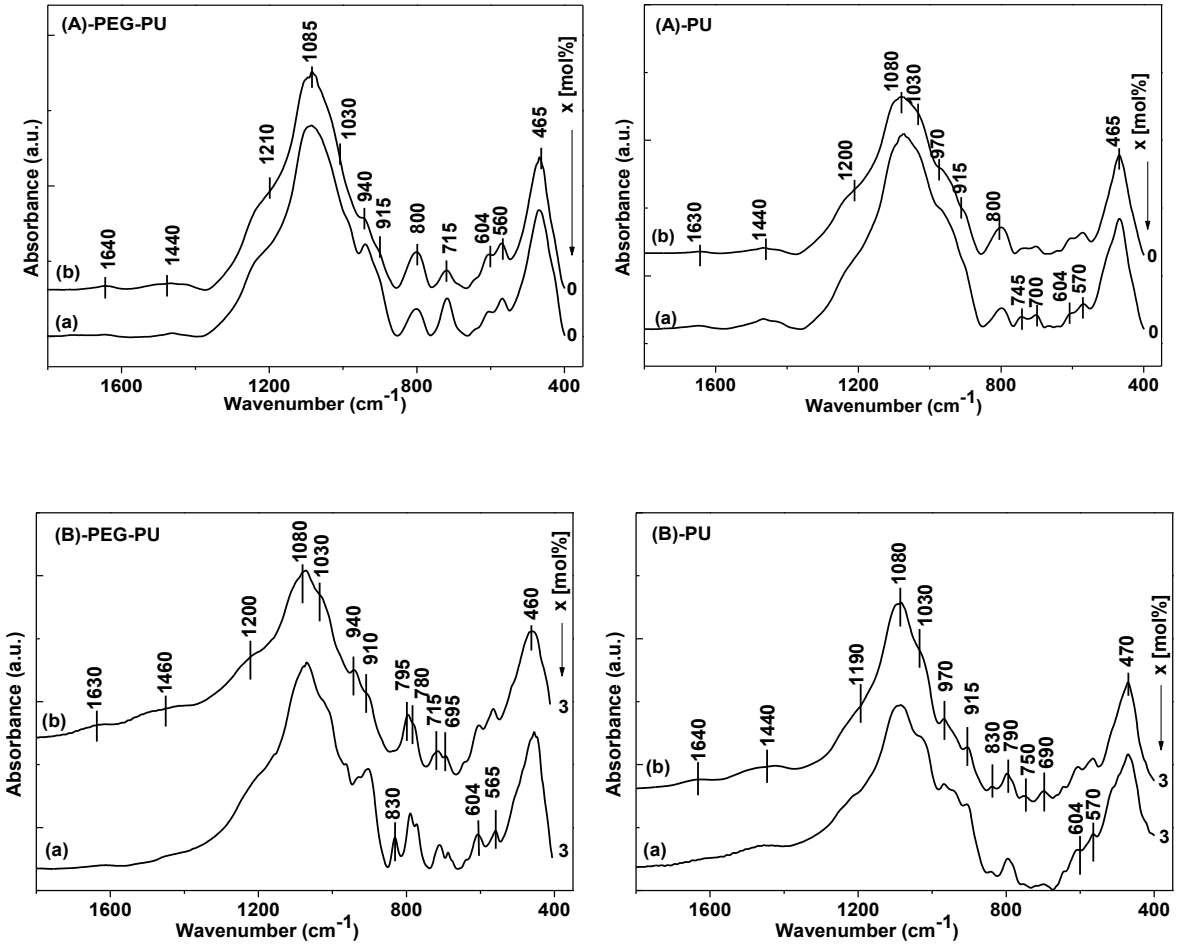

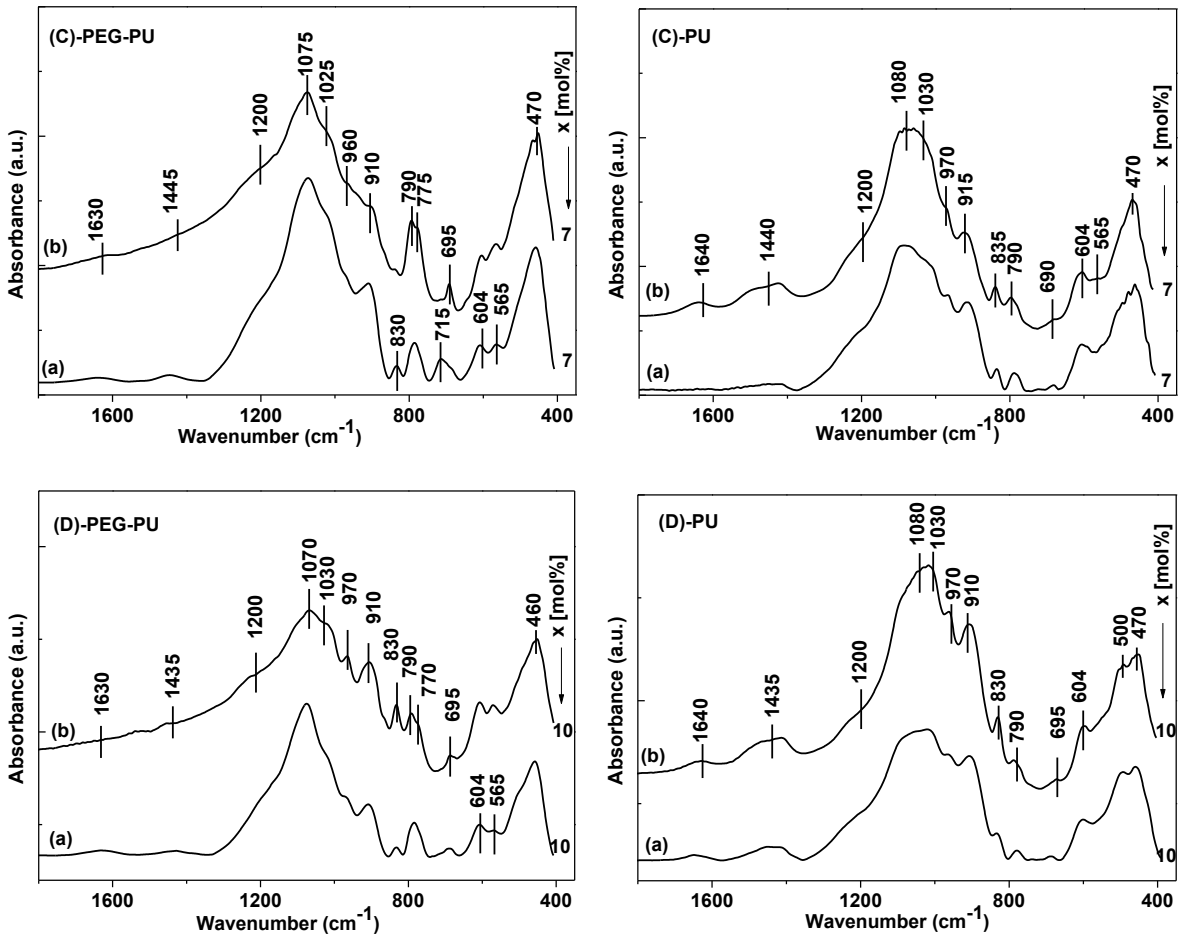

Figure 4.9 FT-IR spectra of the PEG containing and PEG-free scaffold with 0% ZnO (A), 3% ZnO (B), 7% ZnO (C) and 10% ZnO (D) , before (a) and after (b) 14 days of immersion in SBF.

4.6.3 Scanning Electron Microscopy

SEM images taken after 14 days immersion in SBF from samples prepared with PEG (Figure 4.10) reveal the occurrence on their surface of needle shape agglomerates that is a good proof for hydroxylapatite like phases self-assembling in SBF.

At the same time, the post immersed PEG-free sample surface with the highest zinc content is completely free of agglomerates, result confirmed by X-ray diffraction and infrared spectroscopy. It can be concluded from the SEM images that larger amount of zinc in the PEG-free glass-ceramic composition has an inhibitory effect for hydroxylapatite formation. On the other hand, the polymer addition during samples synthesis has favored the formation of apatite layer on their surface even for the highest zinc content.

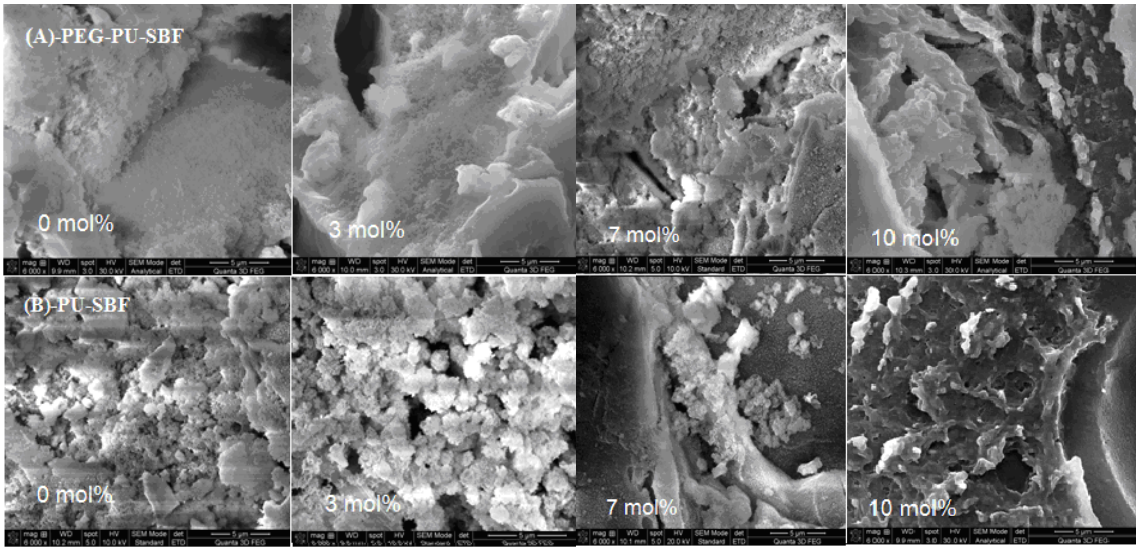

Figure 4.10 Microstructure for the obtained scaffolds with (A-PEG-PU) and without (B-PU) PEG, after 14 days of immersion in SBF

4.7 Cells biocompatibility

Cell viability tests were performed in order to asses the cells cultivated on the prepared samples. One can observe that the viable cells are colored in green and non-viable cells colored in red by using double staining with fluorescein diacetate (1 µg/ml) and propidium iodide (5 µg/ml) as probes (Figure 4.11). The results indicate that cell viability decrease with the increase of the zinc concentration in the glass-ceramic samples prepared both with and without PEG.

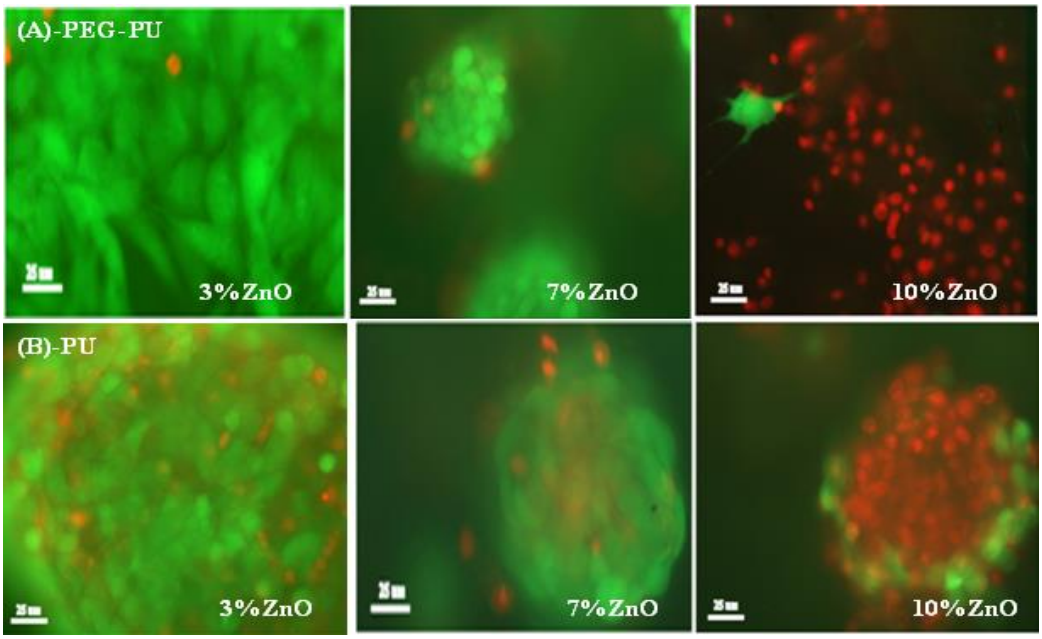

Figure 4.11 Fluorescence micrographs of cell viability cultured on the prepared samples

4.8 Conclusions

- Macroporous zinc containing glass-ceramic scaffolds were successfully prepared by sol-gel synthesis combined with sacrificial template method.
- The PEG addition during sol-gel synthesis influences the morphology of the obtained samples and imparts them greater pore interconnectivity.
- For the glass-ceramic samples resulted after 900^{o}C heat treatment, the main nanocrystalline phases developed in the samples prepared with PEG are pseudowollastonite and hydroxyapatite that favors the increase of the sample bioactivity.
- The *in vitro* tests indicate that the increase of zinc content prevents the hydroxyapatite formation but it has no inhibitory effect in case of the samples prepared with PEG.
- The analysis on *cell cultures* evidence a decrease of cell viability with the increase of zinc concentration.

General conclusions:

Thin films of the new 44.5SiO_2-11ZnO-44.5P_2O_5 (mol %) bioactive glass, were obtained by spin-coating technique. The results indicate that by this technique one can obtain thin films with an inhomogeneous, rough topography with high specific surface area, which is convenient for biomolecules attachment.

Sol-gel derived samples belonging to the 60SiO_2·(35-x)CaO·xZnO·5P_2O_5 system (x = 0, 3, 7, 10 mol %) thermal treatment at 700 ^{o}C, were investigated in order to evaluate the influence of PEG addition on the structural and morphological properties before and after gamma ray irradiation. It was noted for the glasses prepared without PEG that the presence of zinc in the matrix induced resistance to the samples against gamma irradiation, whereas for an increased dose of radiation, Zn^{2+} ions have lost their ability to strengthen the glass sample network. On the other hand PEG addition during samples synthesis has conferred an excellent stability of the glasses against gamma irradiation for sterilization purpose.

The macroporous compounds based on60SiO_2·(35-x)CaO·xZnO·5P_2O_5 with x = 0, 3, 7, 10 mol% glass-ceramic system were prepared following the sol-gel route combined with sacrificial template method and heat treatment at 900^{o}C. The PEG addition during sol-gel synthesis had favorable effect on their bioactivity. The *in vitro* tests indicate that the increase of zinc content prevents the hydroxyapatite formation but it has no inhibitory effect in case of the samples prepared with PEG. Results of *cell culture* analysis also show a decrease of cell viability with the increase of zinc concentration.

5. References:

1. E. Verne, M. Bosetti, C. Vitale-Brovarone, C. Moisescu et al, *Biomaterials*, 23 (2002) 3395.

2. E. Verne, R. Defilippi, G. Carl, C. Vitale-Brovarone, P. Appendino, *J. Eur. Cer. Soc.* 23 (2003) 675.

3. C. Vitale-Brovarone, S. Di Nunzio, O. Bretcanu, E. Verne, *J. Mat. Sci. Mater. Med.* 15 (2004) 209.

4. E. Verne, F. Valles, C. Vitale-Brovarone, S. Spriano, C. Moisescu, *J. Eur. Cer. Soc.* 24 (2004) 2699.

5. C. Vitale-Brovarone, E. Verne, *J. Mat. Sci. Mat. Med*. 16 (2005) 863.

6. M. Yamaguchi, H. Oishi, Y Suketa, *Biochem. Pharmacol*. 364 (1987) 007.

7. G. Lusvardi, D. Zaffe, L. Menabue, C. Bertoldi, G. Malavasi, U. Consolo, Acta Biomater. 5 (2009) 419.

8. L.L. Hench, *J. Mater. Sci. Mater. Med.* 17 (2006) 967.

9. J. Serra, P. Gonzalez, S. Liste, S. Chiussi, L. Leon et al, *J. Mater. Sci. Med*. 13 (2002) 1221.

10. J. Marchi, D.S. Morais, J. Schneider, J.C. Bressiani, A.H.A. Bressiani, *J. Non-Cryst. Solids* 351 (2005) 863.

11. M. Wang, J. Cheng, M. Li, F. He, *Physica B* 406 (2011) 187.

12. M.M. Pereira, A.E. Clark, L.L. Hench, *J. Am. Ceram. Soc.* 78 (1995) 2463.

13. A. Vulpoi, L. Baia, S. Simon, V. Simon, *Mater. Sci. Eng. C* 32 (2012) 178.

14. A. Martinez, I. Izquierdo-Barba, M. Vallet-Regi, *Chem. Mater.* 12 (2000) 3080.

15. J. Simitzis, D.E. Baciu, *Dig. J. Nanomater. Bios.* 7 (2012) 1719.

16. P. Saravanapavan, L.L.Hench, *J. Non-Cryst. Solids*, 318 (2003) 14.

17. R.M. Almeida, G.C. Pantano, *J.Appl. Phys*., 68 (1990) 4225.

18. P. Piao, W.G. Oldham, E.E. Haller, *J.Non-Cryst.Solids*, 276 (2000) 71.

19. A.A. Khan, J.P. Roux, W.J. James, *Acta Crystall. B*, 28 (1972) 2065

20. S. Haimi, G. Gorianc, L. Moimas, B. Lindroos et al, *Acta Biomater*. 5 (2009) 3122.

21. I. Battisha, A. El Nahrawy, *New J. Glass Ceram.* 2 (2012) 17.

22. M.V. Ramachandra Rao, Y. Gandhi, L. Srinivasa Rao, G. Sahayabaskaran, N. Veeraiah, *Mater. Chem. Phys.* 126 (2011) 58.

23. R. Ciceo-Lucacel, O.Ponta, V. Simon, *J. Non-Cryst. Solids* 358 (2012) 2803.

24. M.M. Pereira, A.E. Clark, L.L. Hench, *J. Am. Ceram. Soc*. 78 (1995) 2463.

25. C.Y. Kim, A. E. Clark, L. L. Hench, *J. Biomed. Mater. Res*. 26 (1992) 1147.

26. A. Vulpoi, L. Baia, S. Simon, V. Simon, *Mater. Sci. Eng. C* 32 (2012) 178.

27. D.M. Sanders, W,.B. Person, L.L. Hench, *Appl. Spectrosc*. 28 (1976) 1474.

Acknowledgements

I would like to express my deepest gratitude to my supervisor, Prof. Dr. Viorica SIMON for providing me the honor and privilege to work in her research group. Her understanding, consideration, no ending support and personal guidance have provided the basis for this thesis. Also I am grateful to my supervisor, Prof. Dr. Constantin CIUCE from "Iuliu Hatieganu" University of Medicine and Pharmacy, Faculty of Medicine who provided me all the facilities to finish my work.

My sincere gratitude and thanks go to my committee members for proofreading of the thesis: Acad. Octavian POPESCU from Romanian Academy**,** Bucharest, Prof. Dr. Ing. Catalin POPA from Technical University, Cluj-Napoca and Prof. Dr. Ioan ARDELEAN from Babes-Bolyai University, Cluj-Napoca.

I would like to thank Prof. Dr. Simion SIMON for useful discussions, very good advices and excellent collaboration during my research work.

I also want to thank all professors from Faculty of Physics of Babeș-Bolyai University, who imparted their knowledge during my study.

Moreover, I want to thank to all my colleagues from the laboratory for their help and useful discussion.

I would like to express my love and gratitude to my daughter and my husband for their understanding, patience and permanent support during all these years.

Finally I acknowledge the financial support provided from programs co-financed by The Sectoral Operational Programme Human Resources Development, Contract **POSDRU 88/1.5/S/56949**